The Corrosion of Zirconium Under Deep Geological Repository Conditions

David W. Shoesmith and Dmitrij Zagidulin

The University of Western Ontario

nwmo

NUCLEAR WASTE MANAGEMENT ORGANIZATION

SOCIÉTÉ DE GESTION DES DÉCHETS NUCLÉAIRES

Nuclear Waste Management Organization
22 St. Clair Avenue East, 6th Floor
Toronto, Ontario
M4T 2S3
Canada

Tel: 416-934-9814
Web: www.nwmo.ca

The Corrosion of Zirconium Under Deep Geological Repository Conditions

NWMO TR-2010-19

October 2010

David W. Shoesmith and Dmitrij Zagidulin
The University of Western Ontario

Disclaimer:

This report does not necessarily reflect the views or position of the Nuclear Waste Management Organization, its directors, officers, employees and agents (the "NWMO") and unless otherwise specifically stated, is made available to the public by the NWMO for information only. The contents of this report reflect the views of the author(s) who are solely responsible for the text and its conclusions as well as the accuracy of any data used in its creation. The NWMO does not make any warranty, express or implied, or assume any legal liability or responsibility for the accuracy, completeness, or usefulness of any information disclosed, or represent that the use of any information would not infringe privately owned rights. Any reference to a specific commercial product, process or service by trade name, trademark, manufacturer, or otherwise, does not constitute or imply its endorsement, recommendation, or preference by NWMO.

ABSTRACT

Title: **The Corrosion of Zirconium Under Deep Geological Repository Conditions**
Report No.:   **NWMO TR-2010-19**
Author(s):   David W. Shoesmith and Dmitrij Zagidulin
Company: The University of Western Ontario
Date: October 2010

Abstract
Zirconium alloys are widely used in nuclear reactors as fuel cladding and as reactor structural elements (i.e., CANDU reactor pressure tubes), and are therefore a component of the waste materials that could be emplaced in a deep geologic repository. For this reason, the corrosion mechanisms and rates for relevant zirconium alloys under repository conditions have been reviewed. Since titanium and zirconium alloys have many similarities, and because the data base for the corrosion of titanium alloys under repository conditions is considerably more extensive than that for zirconium alloys, the electrochemical and corrosion behaviour of both materials have been compared and evaluated. Although electrochemical studies suggest Zircaloy cladding could be susceptible to pitting, redox conditions within a failed waste container will remain reducing and unable to support this corrosion process. This leaves passive corrosion as the only corrosion mechanism. The available data indicates that the rate of passive corrosion will be very low. A conservative upper limit for the passive corrosion rate would be 20 nm/year and a reasonable value would be 5 nm/year, although some studies exist to show rates less than 1 nm/year are likely.

TABLE OF CONTENTS

LIST OF TABLES

LIST OF FIGURES

1. INTRODUCTION

Zirconium alloys are widely used in nuclear reactors as fuel cladding and as reactor structural elements (i.e., CANDU reactor pressure tubes). They have been chosen for in-reactor operations because of their combination of a low neutron cross section and corrosion resistance. Minor changes in composition and microstructure can have significant effects on these properties. For fuel cladding applications the alloys of choice are Zircaloy-2 (Zr-2) and Zircaloy-4 (Zr-4), the latter being the material used in current CANDU designs. For CANDU reactors, the pressure tubes are constructed from zirconium containing 2.5% niobium (Zr-2.5Nb) (early reactors used Zr-2). The compositions of these alloys are given in Table 1.

Table 1: The Composition (Mass %) of Zircaloys According to ASTM Specifications

Alloying Elements	Zircaloy-2	Zircaloy-4	Zr-2.5Nb
Sn	1.2 - 1.7	1.2 - 1.7	-
Fe	0.07 - 0.20	0.18 - 0.24	-
Cr	0.05 - 0.15	0.07 - 0.13	-
Ni	0.03 - 0.08	-	-
Nb	-	-	2.5 - 2.8

For the fuel cladding Zircaloys, the primary alloying addition is Sn, an alpha-phase stabilizer added primarily to improve corrosion resistance. Small amounts of Fe, Ni and Cr are also included for similar purposes. These elements tend to separate into the intermetallic compounds, Zr (Ni, Fe) and Zr (Cr, Fe)$_2$. In Zr-4, the Fe content is slightly higher and the Ni content reduced to zero compared to Zr-2, primarily to decrease the adsorption of hydrogen by avoiding Ni, which can act as a catalyst for H absorption.

For use in pressure tubes, alloying with Nb stabilizes the β phase along the grain boundaries of the α-Zr matrix and enhances the corrosion resistance while increasing the strength. The small amount of Fe impurity present in this alloy is found predominantly in the β phase, and does not separate to produce intermetallic compounds.

During in-reactor service, the Zr alloys are exposed to irradiation. For example, CANDU fuel cladding receives neutron fluencies of around 10^{25} neutrons/m^2 (Truant 1983). This irradiation leads to the formation of neutron activation products, such as ^{14}C, ^{59}Ni, ^{63}Ni and ^{93}Zr in fuel cladding, and ^{94}Nb and ^{93}Zr in pressure tubes. Although present in low concentrations, these radionuclides may be released from the Zr alloys as a result of corrosion and therefore need to be considered as part of the long-term safety assessment of any repository containing these materials. A complete listing of cladding activation products and their concentration in the cladding is given elsewhere (Tait et al. 2000). Due to the relatively low temperature it experiences during irradiation (< 400°C), no significant diffusive transport occurs within the Zr, and these activation products are likely to be uniformly distributed throughout the alloy.

During in-reactor irradiation the Zr alloys undergo a number of changes. Corrosion by reaction with water

$$Zr + 2H_2O \rightarrow ZrO_2 + 2H_2 \tag{1}$$

leads to the formation of a relatively thick surface oxide (~4 μm) and the absorption of a considerable amount of hydrogen into the alloy. As-fabricated cladding has a residual H concentration of ~25 μg/g (Tait et al. 2000) which increases to ~100 μg/g (mainly as deuterium) after in-reactor exposure. On removal from reactor, this H(D) precipitates as zirconium hydride as the cladding cools, resulting in embrittlement and an increased susceptibility to fracture.

This report will review the potential corrosion processes that could occur on Zr alloys under deep geologic repository conditions. The discussion will focus primarily on fuel cladding Zr, but will be extended to pressure tube Zr as noted. Since the corrosion performance of titanium and zirconium alloys have many similarities, as well as some instructive differences, both will be considered. The corrosion performance of Ti and its alloys has been studied under geological repository conditions since they have been considered as potential engineered barrier materials, and a number of detailed reviews of their corrosion performance have been published (Shoesmith and Ikeda 1997; Hua et al. 2004, 2005; Shoesmith 2006). Information from these studies on Ti alloys enables a much more definitive review of Zr alloys whose corrosion behaviour under deep geologic conditions has not been studied in significant detail.

2. THE ELECTROCHEMICAL PROPERTIES OF TITANIUM AND ZIRCONIUM ALLOYS

Both Ti and Zr alloys are commonly used in industrial applications where corrosion resistance to aggressive environments is required (Schutz and Thomas 1987, Been and Grauman 2000, Shoesmith and Noël 2010). Both bare metals spontaneously oxidize to produce a thin, chemically inert, oxide film which renders the metal passive and unreactive. While both passivated metals (and alloys) are very stable, the properties of their protective oxides are different and this confers some differences in corrosion properties on the two materials. The oxide film on Ti is a semiconductor with a wide band gap of 3.05 eV and slight deviations from stoichiometry (TiO_{2-x}) give the oxide film n-type characteristics (Torresi et al. 1987). These n-type characteristics can be attributed to a combination of O vacancies and interstitial Ti^{III} ions which lead to the trapping of electrons in a band orbital just below the conduction band edge (Jarzebski 1973, Shoesmith and Ikeda 1997). By contrast, ZrO_2 is an insulator with a very large band gap (> 5 eV) (Meisterjahn et al. 1987).

Electrochemically-determined polarization curves (Noël et al. 2008), Figure 1, show that both metals display a wide passive potential region within which they are electrochemically inert and, hence, corrosion resistant. However, when polarized to positive (anodic) or negative (cathodic) potentials, both materials exhibit significant loss of passivity. At positive potentials, Zr loses passivity more readily than Ti exhibiting substantial current for potentials ≥ 1.3V (vs the Saturated Calomel Electrode (SCE)), while at more negative potentials, Ti more readily supports the cathodic reduction of H_2O at potentials ≤ 1.5V (vs SCE), Figure 1.
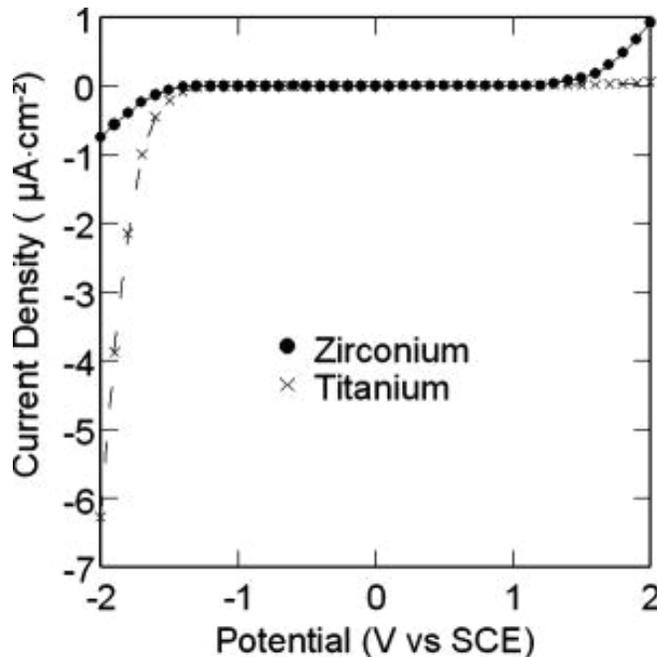
Figure 1: Polarization behaviour of Ti and Zr in neutral 0.1 mol/L KClO$_4$ solution (Noël et al. 2008)

For both metals, anodic polarization leads to oxide growth, but the nature of the growth process and the properties of the oxides are different. For both metals the anodization ratio (increase in oxide thickness per volt applied) is similar, a value of ~2.5 nm/V being obtained for Ti (Tun et al. 1999) compared to 2.8 nm/V (Meisterjahn et al. 1987) to 3.4 nm/V (Noël et al. 2008) for Zr. The differences in film growth behaviour can be explained by the differences in growth mechanism. Anodic films on Zr are crystalline (Cox 1970, Leach and Pearson 1988, Ortega and Siejka 1982), while those on Ti are initially amorphous and undergo potential-induced crystallization only at high potentials (Shibata and Zhu 1995).

Oxidization of Zr is dominated by the migration of oxygen to the metal oxide interface leading to a stress build up at this interface as a consequence of the large Pilling-Bedworth (P-B) ratio of ~1.5 (Noël et al. 2000). (The P-B ratio is the ratio of the volume of oxide created to the volume of metal consumed). This leads to a stress-induced crystallization and the introduction of migration pathways most likely along crystalline grain boundaries (Cox 1970). For Ti, even though the Pilling-Bedworth ratio is even larger (1.72; Tun et al. 1999), stress-induced crystallization does not occur. This can be attributed to the fact that both anion and cation transport occur during oxide growth, the transport numbers being 0.65 and 0.35, respectively (Khalil and Leach 1986). Growth under these conditions avoids stress build-up since the volume of the oxide grown at the metal/oxide interface is just sufficient to replace the volume of metal converted, the remaining oxide growth occurring at the oxide/solution interface where stress-free expansion is possible.

The consequences of these differences can be seen in in-situ neutron reflectometry experiments conducted with the metal under electrochemical control. Anodic oxidation of Ti

results in the formation of a dense rutile structure with H only present in the outer region of the film at the oxide/solution interface (Tun et al. 1999), Figure 2. X-ray photoelectron spectroscopic analyses indicate the H is in the form of OH^- ions or H_2O. These results demonstrate that, for Ti, while incorporation of OH^-/H_2O occurs under oxidizing conditions, it is confined to a layer of $TiO_2 \cdot H_2O$ at the oxide/solution interface. At the metal/oxide interface a dense, protective layer of rutile, similar in properties to that formed by air exposure, persists.
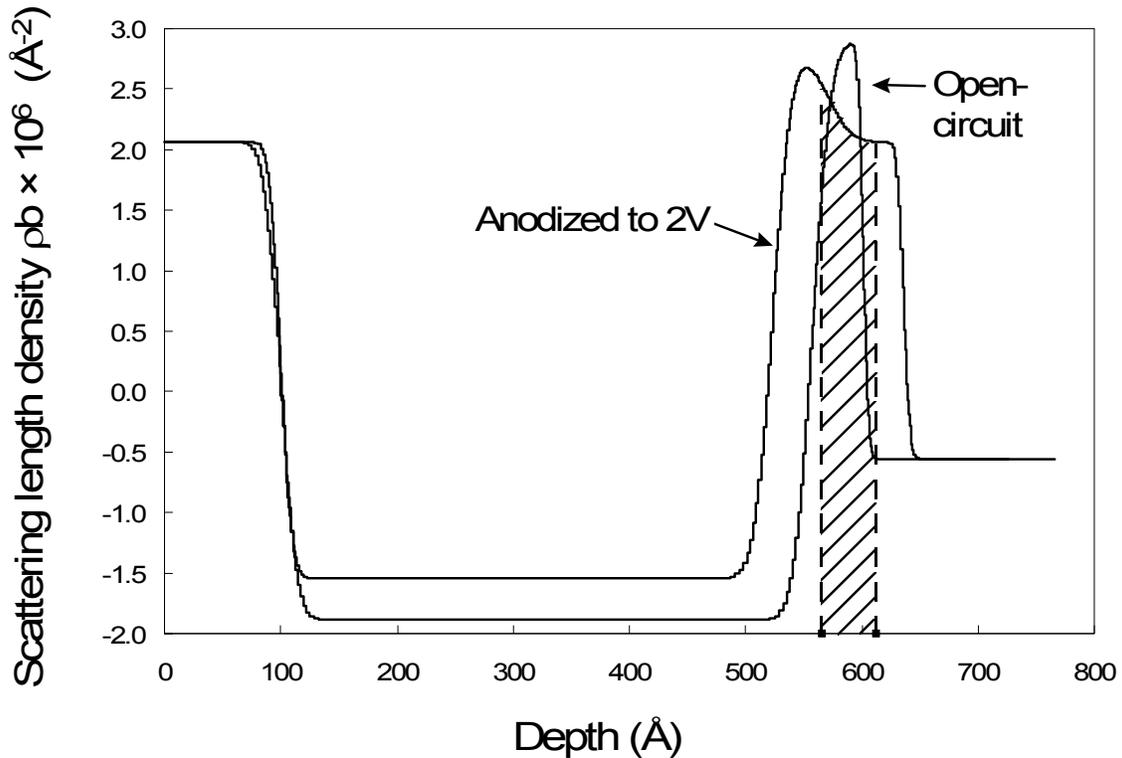
Figure 2: Neutron reflectometry profiles (expressed as the scattering length density (SLD), an indicator of composition) showing the distinct layers comprising the electrode: 0 to ~100Å, the Si wafer substrate; 100 to ~500Å, the sputtered Ti layer; ~500Å to ~650Å, the air-formed oxide film (open circuit) and the film grown anodically at an applied potential of 2V; ≥ 650Å, the aqueous electrolyte solution (neutral 0.27 mol/L NaCl). The shaded region shows the expected position of the original air-formed oxide within the anodically grown film (Tun et al. 1999)

By contrast, similar experiments on Zr, again initially covered by an air-formed oxide, show that under anodic oxidizing conditions, the film, while remaining intact and protective, incorporates OH^-/H_2O throughout the film including in the "dry" air-formed oxide initially present, Figure 3 (Noël et al. 2008). Figures 4 and 5 show the increase in oxide thickness and decrease in neutron scattering length density (SLD), respectively, as the oxidation potential is increased. The SLD is indicative of the composition and density of the film, and the decrease in SLD as the applied potential is made more positive indicates the incorporation of H, an atom with a negative SLD. These neutron experiments show that even a small change in oxidation potential

changes the properties throughout the full depth of the oxide on Zr. Accompanying impedance measurements show that, despite the steady decrease in SLD indicating a potential-dependent increase in OH^-/H_2O content of the film as the potential is made more oxidizing, Figure 5, there is no loss in protectiveness of the oxide due to the introduction of these H_2O-containing migration pathways until the potential reaches 1.5V. When this potential is reached or exceeded, loss of protectiveness is clearly visible as a sudden further increase in OH^-/H_2O (decrease in SLD), Figure 5.
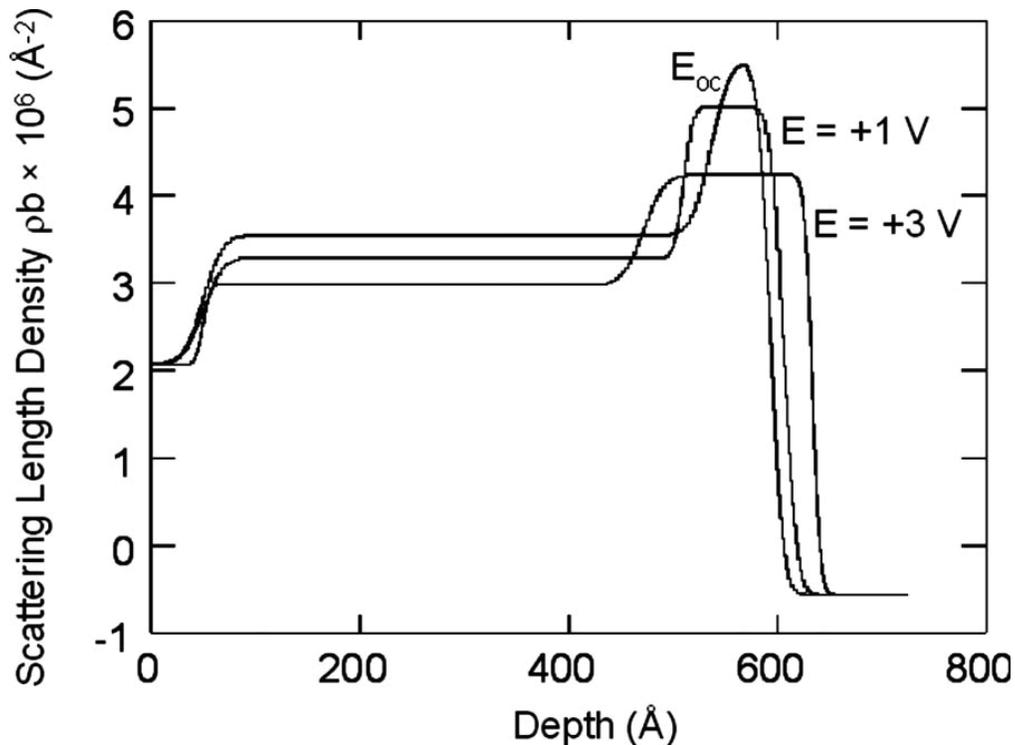
Figure 3: Neutron reflectometry profiles recorded on a Zr electrode showing similar layers to those identified in Figure 2 for Ti. The profile for the air-formed film present on open-circuit is marked E_{OC}. The other two profiles were obtained after anodic oxidation at 1V and 3V (vs SCE), respectively. The decrease in SLD in the oxide as the applied potential is increased indicates an increase in hydrogen content with increasing oxide growth. The constant SLD throughout the oxide indicates the presence of H throughout the film from the metal/oxide interface (at ~45Å (3V)) to the oxide/electrolyte solution interface (at ~650Å (3V)) (Noël et al. 2008)
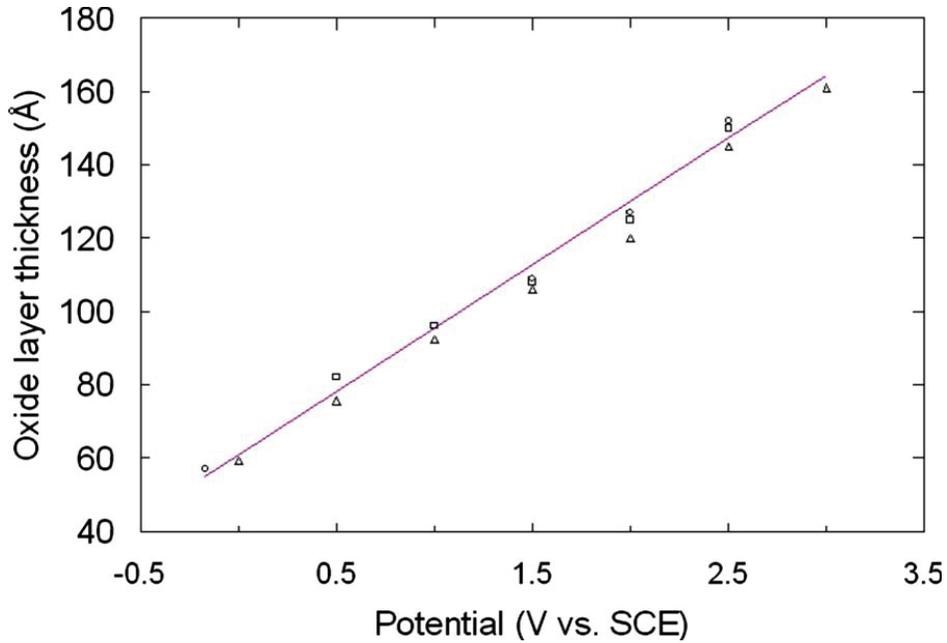
Figure 4: Oxide layer thickness, determined in neutron reflectometry experiments, as a function of applied potential on Zr in a neutral 0.1 mol/L Na$_2$SO$_4$ solution. The symbols, Δ □ ○ show that, while a slight thickening of the oxide occurs with time (6, ~12, ~18 hours, respectively) the thickness has almost achieved a steady-state value (Noël et al. 2008)
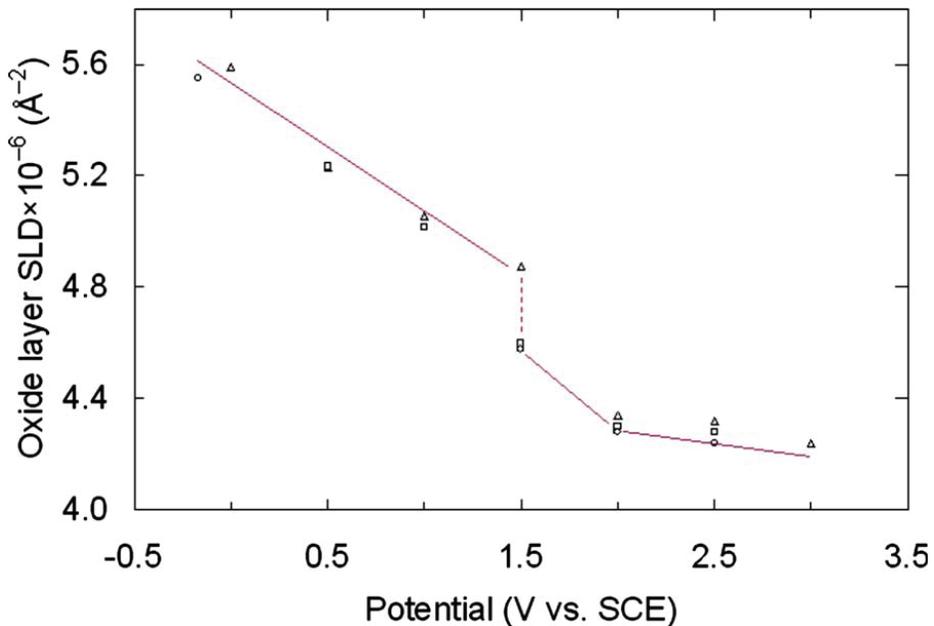
Figure 5: The scattering length density (SLD) of the oxide film on Zr determined by neutron reflectometry after anodic oxidation at various applied potentials. The data points have the same significance as in Figure 4. The decrease in SLD shows that the hydrogen content of the oxide increases steadily as the potential increases up to ~1.5V, and then suddenly increases as the film undergoes fracture (Noël et al. 2008)

These differences in film growth between the two materials are consistent with expectations based on the cation/anion transport numbers. Given the known crystalline nature of the ZrO_2 film, it can be concluded that Zr, but not Ti, contains pathways (crystalline grain boundaries, tight flaws and/or pores) along which water soluble species can migrate. As will be discussed below such a difference can explain why Zr alloys are more susceptible to pitting than Ti alloys.

Under cathodic polarization the two metals also exhibit significant differences, Figure 1. Figures 6 and 7 (Noël et al. 2008) show the film resistances, determined by impedance spectroscopy, as the electrode is polarized to increasingly negative potentials. When comparing these two sets of behaviour, it should be noted that only the relative changes matter, not the absolute values. The latter vary due to differences in electrode pretreatment. For Ti, the film resistance begins to decrease for E ≤ -0.3V (vs SCE) while that for Zr does not vary significantly until E < -1.54V (vs SCE). These values are close to the flatband potentials of -0.54V for Ti (Torresi et al. 1987) and ~ -1.5V (vs SCE) for Zr (Meisterjahn et al. 1987). The discrepancy in the case of Ti will be discussed below. The flatband potential is that potential at which the Fermi level in the oxide equals the redox potential in the solution and no charge (in the form of electrons) crosses the oxide/solution interface. When the potential is made more negative than the flatband value (for an n-type semiconductor) the oxide becomes degenerate and behaves like a metal allowing electron transfer to reduce H_2O to H_2 (in the present case).
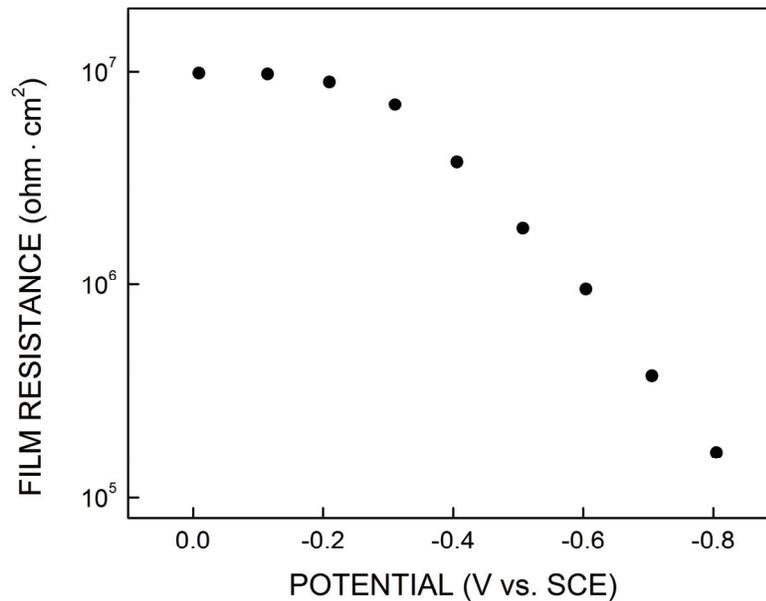
Figure 6: Variation of the oxide film resistance on Grade-2 Ti as a function of applied potential in a deaerated neutral 0.27 mol/L NaCl solution. The resistance was determined by electrochemical impedance spectroscopy on an oxide pre-grown by anodic oxidation at 0.6V (vs SCE) for 48 hours (Zeng 2009)
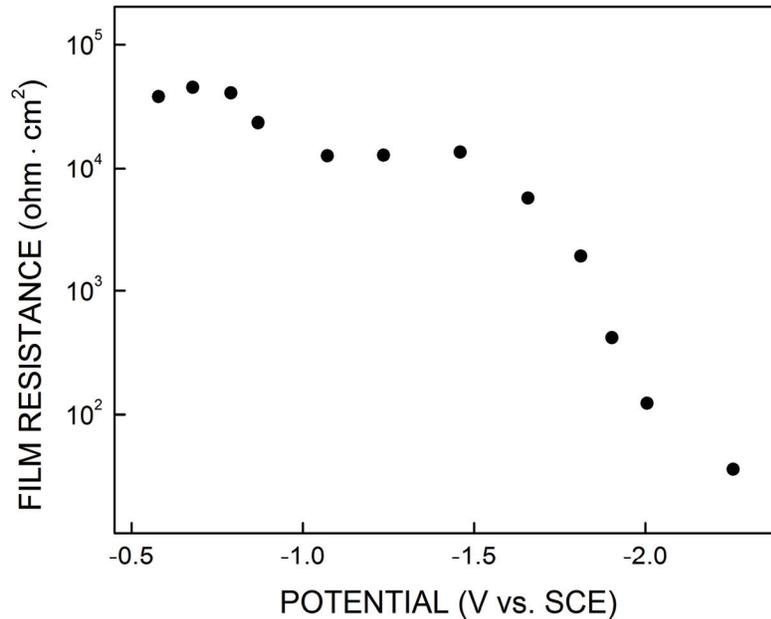
Figure 7: Variation of the oxide film resistance on Zr-2 as a function of applied potential in a deaerated neutral 0.1 mol/L Na$_2$SO$_4$ solution. The resistance was determined by electrochemical impedance spectroscopy on an oxide pre-grown in air for 24 hours prior to exposure to the solution (Nowierski et al. 2009a, b)

For TiO$_2$ on Ti, once the potential is polarized negative to the flatband value, the oxide undergoes redox transformations (Ti^{IV} → Ti^{III}) leading to the availability of multiple oxidation states and a consequent increase in conductivity. This facilitates electron transfer across the oxide/solution interface to reduce H$_2$O, a process accompanied by the absorption of H into the oxide as clearly demonstrated by neutron reflectometry (Tun et al. 1999) and illustrated schematically in Figure 8. This coupled redox transformation-hydrogen absorption process can be described by the reaction (Ohtsuka et al. 1987)

$$TiO_2 \; + \; xH^+ \; + \; xe^- \rightarrow TiO_{2-x}(OH)_x. \tag{2}$$
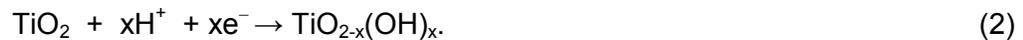
For Zr, similar redox transformations are unavailable and the very negative flatband potential means degeneracy, leading to a reduction in film resistance and the onset of H$_2$O reduction, is not achieved until ~ -1.5V, Figure 7. The absence of changes in film properties and further incorporation of H has been demonstrated by neutron reflectometry to potentials as negative as -2.5V, Figure 9.

Water Reduction

H_2O H_2

Aqueous Environment

Passive Oxide

O^{2-} H_{abs}

Oxide Growth

Ti^{4+} TiO_2 TiOOH   Oxide Transformation

H^-

Ti TiH_x

Metal Oxidation   Hydride Formation   Metal
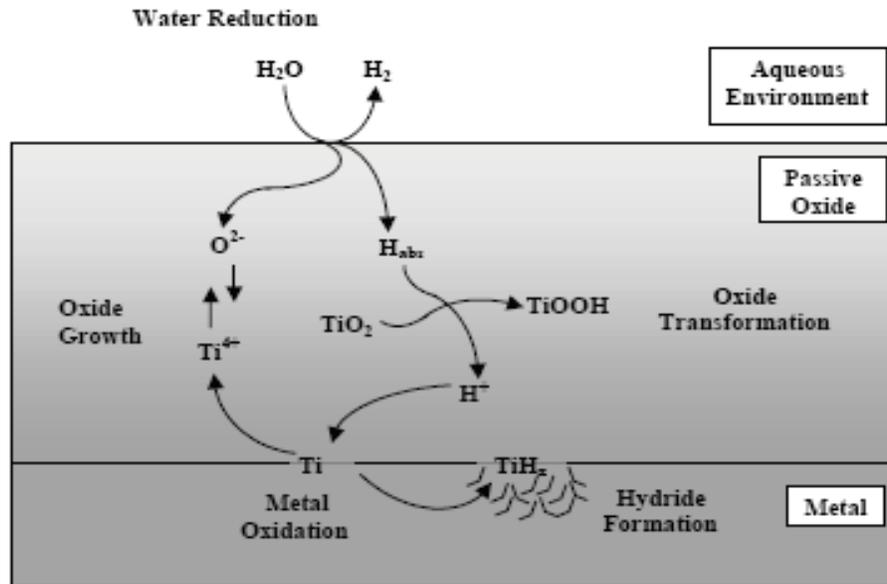
Figure 8: Schematic illustration of the transformations in a TiO$_2$ film on Ti occurring under cathodic polarization leading to the absorption of H into the metal and the formation of hydrides

Commercial Ti and Zr alloys inevitably contain small concentrations of alloying elements and impurities with limited solubility in the α-Ti or α-Zr matrix. As a consequence, they segregate to grain boundaries to form intermetallic precipitates; e.g., Fe-containing β-phase and Ti_xFe in commercially pure Ti (Grade 2; Ti-2), Zr_2 (Fe, Ni) and Zr (Fe, Cr)$_2$ in Zircaloys, and Nb-stabilized β phase in Zr-2.5Nb. The presence of secondary phase precipitates (SPPs) in Zircaloys does not have a major influence on the passive behaviour except at the extremes of anodic and cathodic polarization.

This influence has recently been studied using scanning electrochemical microscopy (SECM), a technique able to probe the reactivity of individual locations on a surface with a resolution of a few microns (Zhu et al. 2007, 2008; Nowierski et al. 2009a). This is achieved by measuring the electrochemical consumption of a redox reagent, dissolved in the solution, on the alloy surface using a microelectrode, located within a few microns of the surface, to measure the current required to regenerate the consumed mediator. By scanning the microelectrode through the solution above the substrate, the reactivity of an area of the surface can be mapped.
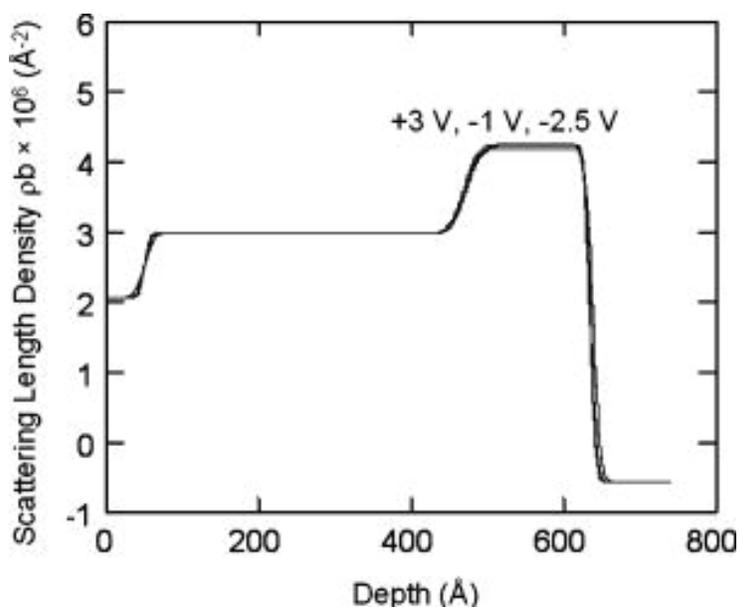
Figure 9: Neutron reflectometry profiles recorded on Zr as a function of applied potential in a neutral 0.1 mol/L Na_2SO_4 solution. The electrode was oxidized at a series of increasingly positive potentials up to +3V (profile shown). Subsequently, the anodically oxidized electrode was cathodically polarized to a series of more negative potentials (the profiles for -1V and -2.5V are shown). The similarity of the profiles shows that no significant change in the composition of the oxide occurs as a consequence of cathodic polarization (Noël et al. 2008)

Figure 10 shows a series of such images recorded at a single location on Ti-2 as the applied potential is made increasingly negative. A number of locations become more easily activated than the general oxide-covered surface. The black lines are drawn to interconnect these locations and their pattern is similar to that of the grain boundaries, indicating that it is the Ti_xFe precipitates at these locations which are preferentially activated. This activation occurs at potentials ~250 mV above the flatband potential, making these locations preferential sites for H_2O reduction compared to the passive oxide-covered α-matrix. Also, given the ability of these secondary phases to absorb H, they are also potential windows for H absorption into the alloy providing the corrosion potential can be polarized to these potentials under natural corrosion conditions. This process is illustrated in Figure 11.

Similar experiments on Zr-2 showed no indication of the activation of grain boundary precipitates and/or β-phase until the potential was ≤ -1.3V, Figure 12 (Nowierski 2009b). These, and the neutron reflectometry results demonstrate the stability of the ZrO_2 film on Zr alloys to cathodic reduction leading to the avoidance of H absorption. Although not studied by these techniques, Zr-2.5Nb would be expected to require potentials at least as negative prior to cathodic activation.
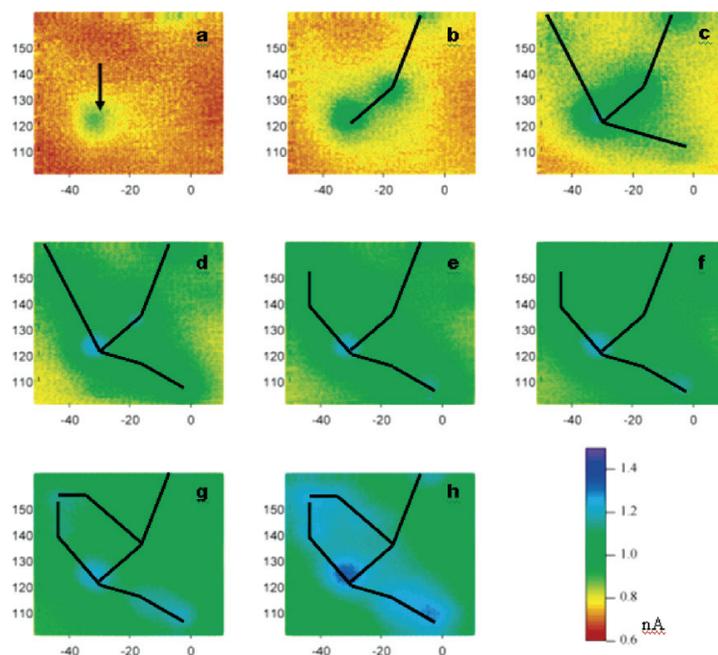
Figure 10: Scanning electrochemical microscopy (SECM) images recorded on a single location on a Ti-2 electrode at various applied potentials in a neutral 0.1 mol/L NaCl solution. The imaged area was 60 µm x 60 µm, and all the images have the same current scale as indicated in the bottom right of the figure. The electrode was allowed to establish a steady-state corrosion potential before application of a series of increasingly negative potentials. The potentials then applied were (in V vs SCE): (a) -0.05; (b) -0.1; (c) -0.15; (d) -0.20; (e) -0.25; (f) -0.30; (g) -0.35; and (h) -0.40V. The initial slightly active spot is indicated by an arrow in (a). As the potential is made more negative new active locations appear. These locations are linked by black lines to indicate grain boundaries (Zhu et al. 2007)

There is also published evidence to show that the presence of these SPPs does not significantly influence the anodic behaviour of either Ti or Zr alloys until the potential is polarized to values > 1V (Casillas et al. 1994, Ito and Furuya 1996). For both Ti and Zr alloys, activation of SPPs leads to the oxidation of H_2O to O_2. In the case of Ti, the presence of a thicker oxide film prevents their activation (Casillas et al. 1994) and passivity is maintained. For Zr-2 (and Zr-4) the precipitates become unstable and undergo transpassive dissolution (i.e., the conversion of Cr in the SPP particles, or Cr^{III} in the oxide covering the particles, to soluble Cr^{VI} (CrO_4^{2-})) (Ito and Furuya 1996). A similar durability of the oxide film on Zr-2.5Nb has been demonstrated electrochemically (Jensen 2002).
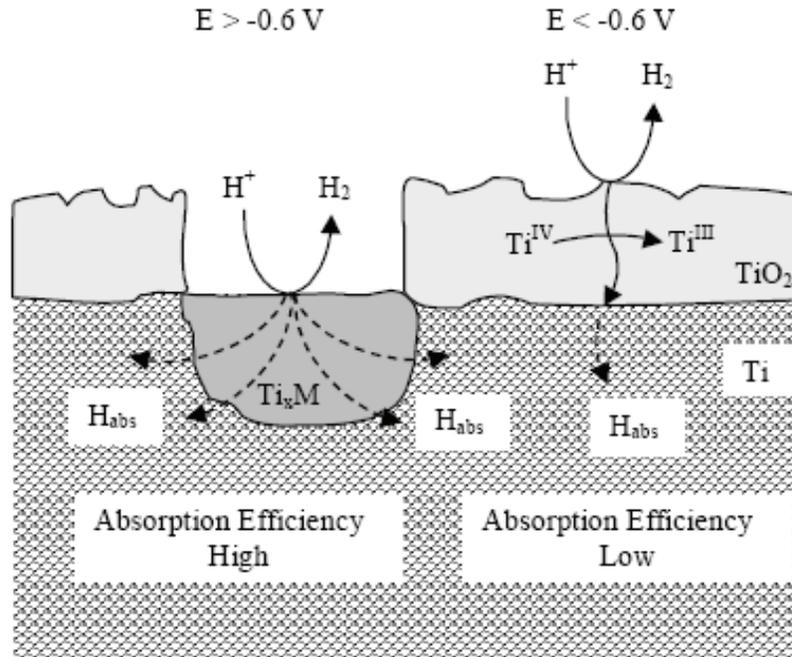
Figure 11: Schematic illustrating the low efficiency of H absorption under passive conditions on Ti and the possibility of a higher absorption efficiency through the locations of cathodically-activated secondary phase precipitates (SPPs)
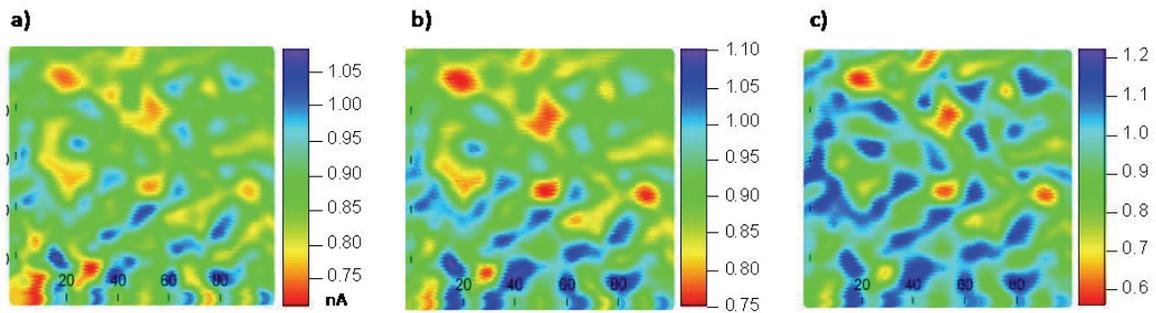
Figure 12: Scanning electrochemical microscopy (SECM) images of the same area on an oxide-covered Zr-2 electrode at various applied potentials in a neutral 0.1 mol/L Na$_2$SO$_4$ solution. The imaged area was 100 µm by 100 µm. The electrode was allowed to establish a steady-state corrosion potential before application of a series of increasingly negative potentials. No cathodically activated locations were observed until the applied potential reached a value of -1.3V (vs SCE). The images show the activation of grain boundary locations at (a) -1.3V; (b) -1.6V; and (c) -1.9V (vs SCE) (Nowierski 2009)

An attempt to summarize these observations is shown in Figure 13. Consistent with the polarization curves shown in Figure 1, the passive film on Ti and its alloys is more resilient under anodic (oxidizing) conditions while that on Zr and its alloys is more resilient under cathodic (reducing) conditions.
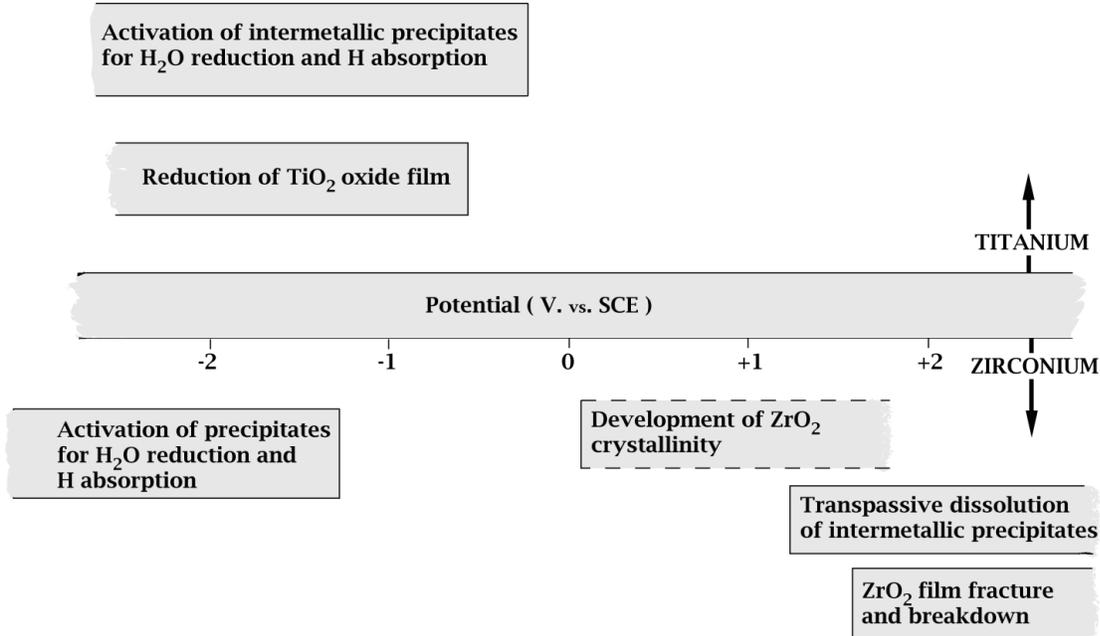
Figure 13: Schematic showing the potential ranges within which various processes can occur on anodically or cathodically polarized Ti and Zr alloys

3. IN-REACTOR OXIDE GROWTH ON ZIRCALOYs AND Zr-2.5Nb

In order to assess the performance of Zr alloys under deep geologic repository conditions, a knowledge of the properties of the film present on discharge from reactor, and how they can be interpreted based on the electrochemical properties discussed above in Section 2, are essential. Here, the in-reactor corrosion process is reviewed with the primary purpose of determining the characteristics and properties of the oxide films formed. Only a brief summary is given, a more detailed review having been published elsewhere (IAEA 1998). While the emphasis is on the Zircaloy cladding, the properties of the film on Zr-2.5Nb are also discussed.

The early stages of oxide formation on Zr and its alloys occur with the metal/oxide interface under compression since oxide growth involves the inward diffusion of O to this interface and the P-B ratio is high (~1.56). As a consequence, in-reactor oxide growth proceeds initially according to a cubic growth law, before the development of fractures and porosity enforces a transition to a faster linear growth process. Correlations of oxidation kinetics with O transport rates within the oxide indicate that O transport occurs primarily along crystallite boundaries (Cox and Roy 1966, Cox and Pemsler 1968).

Electrochemical studies show that oxide growth is driven by a high electric field across the oxide and that the electronic resistivity of the film (i.e., the resistance to the electron transport process required to support H_2O reduction at the oxide/solution interface) has a significant limiting influence on oxide growth (Cox 1969). This last observation indicates that oxidation, and hence corrosion under disposal conditions, could be controlled by the kinetics of the cathodic water reduction reaction if this is forced to occur on the oxide surface.

The evolution from pre- to post-transition growth involves development of a fine porosity, which appears to be induced by tetragonal to monoclinic transformations within the film. Film growth kinetics become effectively linear and involve a series of cyclic events as growth accelerates and slows periodically. Preferential growth of some crystallographic orientations leads to the columnar crystalline morphology eventually observed (IAEA 1998). Impedance and porosity measurements (IAEA 1998) suggest this fine porosity (10 to 100 nm) may penetrate close, if not up, to the Zr/oxide interface, and there is no unequivocal evidence to support the reformation of an oxide barrier layer once the porous structure has developed and post transition kinetics have been established.

In the post transition region, linear growth can be supported by more facile transport processes within the porous structure. There is good evidence from neutron reflectometry studies on anodically grown ZrO_2 films on pure Zr that H_2O can penetrate the oxide film (Figure 3) and it is intuitively reasonable that such a penetration will be more facile at high in-reactor temperatures in the presence of pores.

More recently, more detailed investigations of oxide film properties have been made using transmission electron microscopy (TEM) (Yilmazbayhan et al. 2006) and mass spectrometry (Hutchinson et al. 2007). TEM analyses of the oxide formed on Zr-4 in water (300°C for 784 days) revealed a mixture of tetragonal and monoclinic ZrO_2. The film consisted of layers of columnar and equiaxed grains with a periodic arrangement consistent with the occurrence of a periodic growth - fracturing - regrowth process as discussed previously (Yilmazbayhan et al. 2006, and references therein).

Examination of the region close to the alloy/oxide interface showed a complicated structure. The TEM study suggested the microstructure described above extended to the alloy/oxide interface suggesting no barrier layer was present. An oxide gradient was observed in the alloy surface indicating O diffusion into the metal to form a suboxide. Within this suboxide, the O level exceeds the ~29% solubility level for O in α-Zr, leading to the precipitation of small ZrO_2 crystallites. For oxides grown on Zr-2 (500°C for 144 hours), mass spectrometry measurements (Hutchinson et al. 2007) showed that, while the film at the oxide/solution interface was stoichiometric ZrO_2, an O concentration gradient was present over a 150 nm to 400 nm region close to the Zr-2/oxide interface, indicating a composition approaching ZrO at the interface. Such a region suggests the presence of a barrier layer not detected in the TEM studies. An electrochemical impedance study on Zr (0.25 Sn : 0.11 Fe : 0.01 Cr : 0.01 Ni (wt%)) in 0.1 M $B(OH)_3$ containing 0.001 M LiOH (at 250°C) was similarly inconclusive (Ai et al. 2008). Despite assuming in the modeling of the impedance data that a barrier layer was present, the results indicated that the corrosion resistance was dominated by the porosity of the outer layer.

In the study on Zr-4 (Yilmazbayhan et al. 2006), the oxidation front was found to bypass the secondary phase precipitates (SPP) (Zr_2 (Fe, Ni) and Zr (Fe, Cr)$_2$) leading to their incorporation into the oxide in unoxidized form. Many metallic SPPs were observed in the oxide near the

alloy/oxide interface, but beyond a certain distance from the interface they existed in the oxidized form. The size and distribution of SPPs in Zircaloys have been shown to influence in-reactor corrosion kinetics (IAEA 1998) and electrochemical evidence exists to demonstrate they act as preferential cathodes. Other studies have also demonstrated that their oxidation rate is lower than that of the matrix Zr, leading to a decrease in in-reactor corrosion kinetics (IAEA 1998).

The influence of SPPs on H profiles in the oxide film has been demonstrated by SIMS (Hatano et al. 1996). By comparing the amount of H in the films on steam oxidized Zr-2 containing either fine or coarse-grained SPPs, it was demonstrated that their retention in the unoxidized form in the oxide matrix (as was the case for the coarse-grained precipitates) increased the rate of H transport in the oxide. The rate controlling process was transport through the oxide with periods of rapid transport through the unoxidized intermetallics, which, as a consequence of their 3-d metal content, have a large affinity for H (e.g., $Zr (Fe, Cr)_2$ intermetallics can absorb H up to a composition of $ZrFeCrH_3$ (Shaltiel et al. 1977)).

As long as the SPPs remain unoxidized in the metallic state in the oxide film they can facilitate both electron and H transport. Also, their corrosion leads to the doping of the associated oxide with subvalent cations (Fe^{III}, Cr^{III}, Ni^{II} in a Zr^{IV} lattice). This leads to an increase in the number of O vacancies which act as holes to increase the electronic conductivity of the ZrO_2, again enabling such locations to act as preferential cathodic locations.

An attempt to summarize (in simplified form) the various properties of the oxide film present on Zircaloy cladding is shown in Figure 14. The following features can be identified:

(1) a region within the α-Zr matrix containing dissolved O;
(2) a thin ZrO_2 barrier layer with a depleted O content at the alloy/oxide interface;
(3) an outer columnar, crystalline ZrO_2 oxide film containing a network of pores which allow water access to the barrier layer/outer layer interface;
(4) secondary phase particles (SPPs) isolated in the metallic form in the outer layer oxide matrix which can incorporate large quantities of H and facilitate its transport into the Zircaloy matrix;
(5) SPPs in, or in contact with, the Zircaloy matrix which can also facilitate H transport into the alloy; and
(6) areas of subvalent-doped ZrO_2 with enhanced conductivity produced by oxidation of SPPs.

The evidence in support of a barrier layer under high temperature in-reactor conditions is ambiguous, and it may be that its absence is necessary to sustain the linear oxidation rate observed over longer exposure times. However, on removal from the reactor, when oxide growth is no longer driven by high in-reactor temperatures, a barrier layer will inevitably form at any exposed Zr location. Attempts to measure the barrier layer thickness for post transition oxides (Cox 1968) suggest they are very thin.

The oxidation kinetics of Zr-2.5Nb differ somewhat from those of Zircaloy (IAEA 1998). Often, no clearly defined transition is evident; rather a steady change from cubic to linear kinetics is observed. This behaviour is commonly interpreted as due to the development of porosity from the start of oxidation which reaches a steady-state when the rates of development of porosity and a new barrier layer become equal. This was supported by porosity and impedance measurements which show a similar (but slightly smaller) porosity but a thicker barrier layer (Cox 1987). Since Nb and Zr possess similar oxidation potentials, the rates of oxidation of α-Zr

and Nb-stabilized β phase are similar, the latter being only slightly more rapid. This leads to an oxide which, while slightly more complicated due to the presence of the two phase alloy structure, exhibits a similar microcrystallinity and columnar growth structure to that observed on Zircaloys. In the absence of SPPs, the localized doping of the oxide, leading to enhanced conductivity to support cathodic reactions, is avoided. This, and the impermeability of the thicker barrier layer, leads to a more homogeneous electronic conductivity and a considerably slower rate of hydrogen absorption.
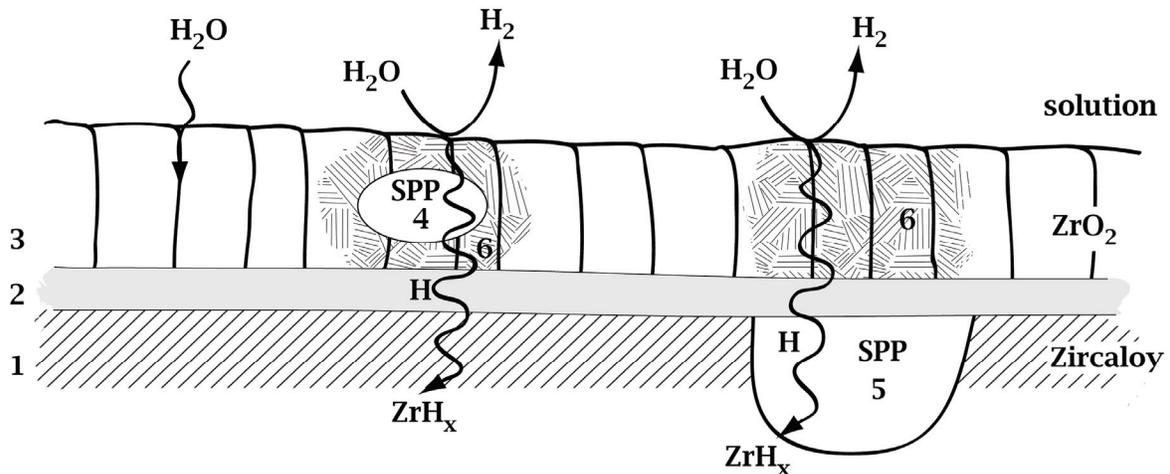
Figure 14: Schematic showing a simplified summary of the various features of oxide films formed in-reactor on Zircaloy and Zr-2.5Nb: (1) O dissolved in the α-Zr matrix; (2) ZrO_2 barrier layer; (3) columnar, crystalline ZrO_2 oxide; (4) unoxidized secondary phase particles (SPP) isolated within the oxide film; (5) SPPs in, or in contact with the Zircaloy matrix; and (6) subvalent-doped ZrO_2 with enhanced electrical conductivity produced by oxidation of SPPs. For Zr-2.5Nb, features (4) to (6) are not present.

4. DEEP GEOLOGIC REPOSITORY CONDITIONS

In a used fuel deep geological repository, used fuel bundles and their associated Zr cladding are encapsulated in durable containers and the containers are sealed in an engineered vault at a depth of hundreds of metres in a stable low permeability rock mass (Garisto et al. 2009). For a repository in a crystalline host rock, the reference design for a Canadian used fuel waste container involves the use of a carbon steel vessel with an outer corrosion barrier of Cu, as illustrated in Figure 15 (Maak 2007). Pressure tubes, which are considered to be long-lived intermediate level waste, will be placed in a deep geologic repository for low and intermediate level waste (Little et al. 2010). However, these tubes would be placed in a different type of container; for example, one based on steel and concrete (Little et al. 2010).

In the event of container failure, the corrosion of, and radionuclide release from, the Zr alloys will depend on the properties of the groundwater and how they are modified by the chemical and corrosion processes occurring within the failed container. Of particular importance will be the groundwater composition, its redox potential and its pH.
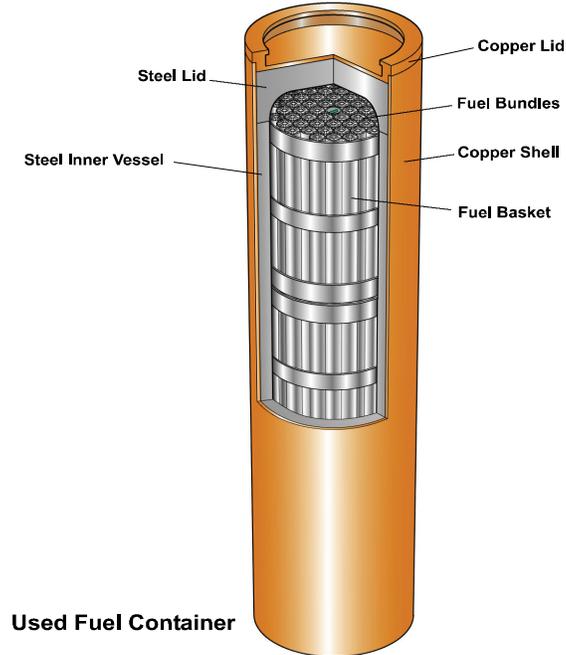
Figure 15: Cut away view of the used fuel container showing the inner and outer vessels and the fuel bundles (Shoesmith 2007)

A set of nominal reference deep groundwaters have been specified for the two potential host rock types of interest: crystalline rock, largely found on the Canadian Shield, and sedimentary rocks, such as those found in the Michigan basin in the Southern parts of Ontario. Several groundwaters have been defined, Table 2. Of these, three are representative of those expected in deep crystalline rock locations: (i) CR-50, typical of groundwaters from depths around 1250 m; (ii) CR-20, typical of groundwaters from depths ranging from 500 to 1000m; and (iii) CR-10, based on the original synthetic groundwater defined for the Whiteshell Research area. Two groundwaters representative of those encountered in deep sedimentary rocks have also been defined: (i) SR-300, a Ca-dominated water typical of samples from depths of around 680m; and (ii) SR-170, a Na-dominated water derived from samples taken from an average depth of about 570m.

Table 2: Reference Groundwater Compositions[*]

Rock Type	Crystalline			Sedimentary	
Water Name	CR-50	CR-20	CR-10	SR-300	SR-170
pH	7.5	7.5	7.5	6.5	6.5
Eh (mV vs SCE)	-440	-440	-440	-440	-440
Solutes (mg/L)					
Na	5,100	3,400	1,900	43,100	37,400
Ca	15,000	4,800	2,130	57,300	14,700
Mg	200	50	60	9,900	3,900
HCO$_3$	10	25	70	40	60
SO$_4$	800	800	1,000	160	460
Cl	34,300	13,800	6,100	199,500	97,400

[*]Not all solutes are shown.

The deep groundwaters are assumed to be reducing and have been assigned an E_h value of - 440mV (vs. SCE) (-200mV vs. SHE), based on the assumption that redox conditions are controlled by the Fe_3O_4/Fe^{2+} equilibrium reaction and that the groundwater pH is effectively neutral. This value of E_h is similar to that adopted in European waste management programs (Wersin et al. 2003, Duro et al. 2006).

Within a failed waste container, the salt content of the groundwater will not change significantly. Under the anoxic conditions established by the incoming groundwater, the carbon steel vessel will react with H_2O to produce Fe^{2+} and H_2 and the corrosion product magnetite (Fe_3O_4),

$$Fe + 2H_2O \rightarrow Fe^{2+} + H_2 + 2OH^- \tag{3}$$
$$Fe + 4H_2O \rightarrow Fe_3O_4 + 4H_2 \tag{4}$$

The corrosion of steel under these conditions will occur at corrosion potentials, E_{CORR}, of ≤ - 800mV (vs. SCE) (-560mV vs. SHE) (Blackwood et al. 1995; Smart et al. 2002a, b; Lee et al. 2005), but would not be expected to disturb the groundwater redox conditions (E_h) significantly, since they were already established by the Fe^{2+}/Fe_3O_4 equilibrium prior to entering the failed container. At the pH of the groundwater (~7.5) the equilibrium solubility of Fe^{2+} would be > 10^{-4} mol/L, Figure 16, but could vary somewhat depending on the extent of hydrolysis of Fe^{2+},

$$Fe^{2+} + yH_2O \rightarrow Fe(OH)_y^{(2-y)+} + yH^+ \tag{5}$$

This influence on pH would not be expected to be large since the protons produced by hydrolysis (reaction 5) will be mainly consumed by OH^- produced by reaction 3 and the concentration of Fe^{2+} would be expected to stay within the range 10^{-4} to 10^{-5} mol/L.
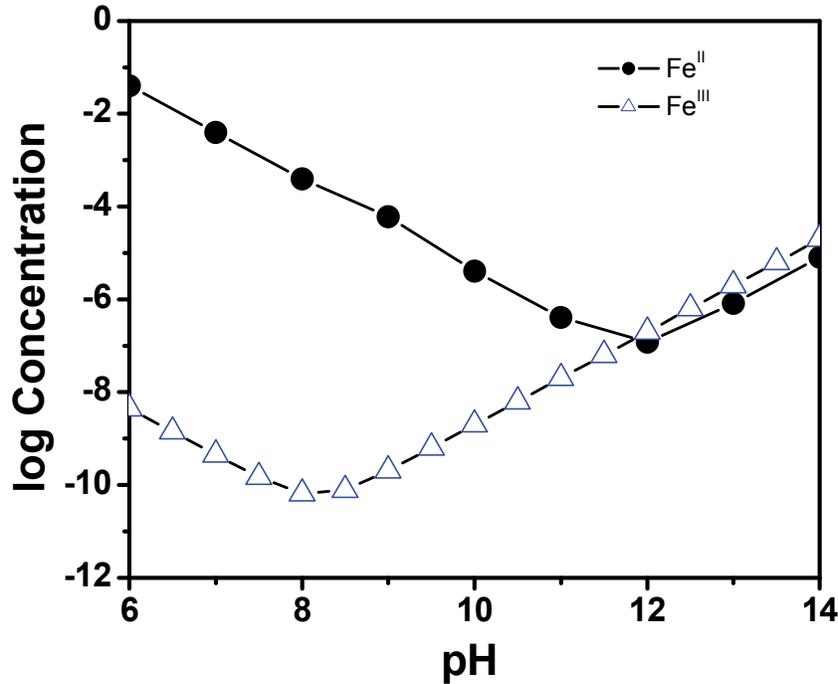
Figure 16: Solubility of Fe^{2+} and Fe^{3+} ions as a function of pH

The primary disturbance of redox conditions could be caused by the radiolysis of water due to the radiation fields associated with the waste. This would be applicable to Zr fuel cladding due to the radiation associated with the used fuel, but would not apply to Zr-2.5Nb pressure tubes.

Figure 17 shows the radiation dose rates to H_2O in contact with a CANDU fuel bundle with a burnup of 220 MWh/kgU (Shoesmith 2007). Two scenarios can be envisaged; intact cladding, when H_2O contacts only its outer surface; and failed cladding when H_2O contacts both inner and outer surfaces. For intact cladding, only gamma radiation is sufficiently penetrating to produce radiolysis products at the outer cladding surface, and beyond a few hundred years gamma dose rates can be considered insignificant. For shorter times, any significant effect of radiolysis on groundwater redox condition will be suppressed by the carbon steel corrosion products. Hydrogen is known to suppress the production of oxidants by gamma radiolysis (Elliott and Bartels 2009) by reactions, such as,

$$H_2 + OH^\bullet \rightarrow H_2O + H^\bullet \tag{6}$$
$$H^\bullet + H_2O_2 \rightarrow H_2O + OH^\bullet \tag{7}$$
$$H^\bullet + O_2 \rightarrow HO_2^\bullet \tag{8}$$
$$H^\bullet + HO_2^\bullet \rightarrow H_2O_2 \tag{9}$$
$$e_{aq} + H_2O_2 + \rightarrow OH^- + OH^\bullet \tag{10}$$
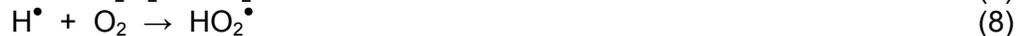
Fe^{2+} also consumes radiolytic oxidants via the Fenton reaction (Jonsson et al. 2007),

$$Fe^{2+} + H_2O_2 \rightarrow Fe^{3+} + OH^\bullet + OH^- \tag{11}$$
$$Fe^{2+} + OH^\bullet \rightarrow Fe^{3+} + OH^- \tag{12}$$

Any Fe^{III} produced in this manner will be precipitated as Fe^{III} solids, since the solubility of Fe^{3+} is many orders of magnitude lower than that of Fe^{2+} in the neutral pH range, Figure 16.
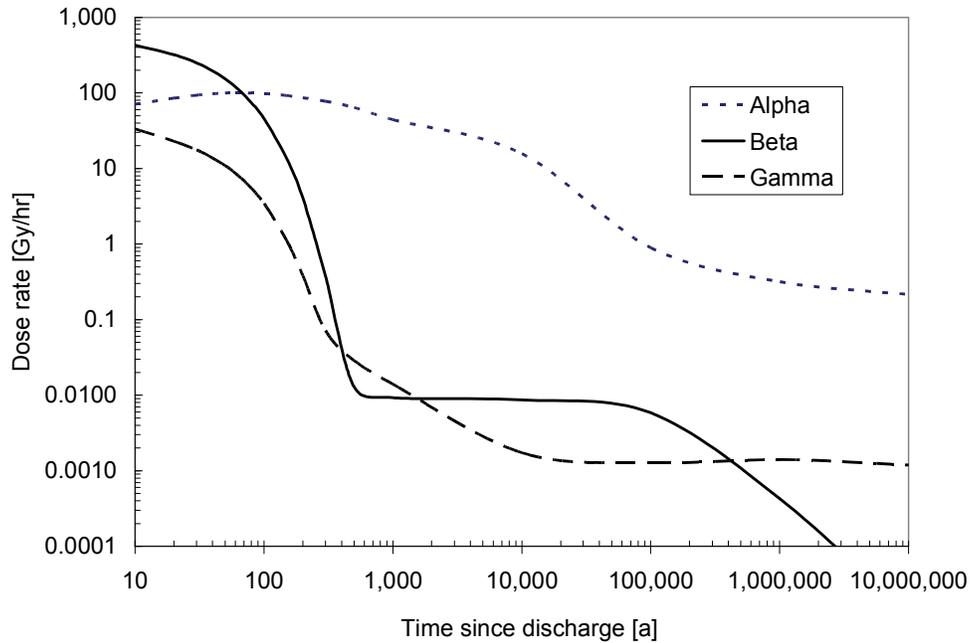
Figure 17: Alpha, beta and gamma radiation dose rates calculated as a function of time for a layer of water in contact with a CANDU fuel bundle with a burnup of 220 MWh/kgU (Shoesmith 2008)

For failed cladding, similar redox scavenging reactions would be anticipated. In this case, α-radiolysis to produce molecular oxidants (primarily H_2O_2), Figure 17, would be most likely to influence groundwater redox conditions. However, there is now a considerable accumulation of evidence to show that even small amounts of H_2 can effectively suppress fuel corrosion inside failed cladding (Shoesmith 2008) primarily by a catalytic process on the surface of the fuel. While, for alpha radiolysis, it is not possible to claim the production of oxidants will be completely suppressed by H_2, any residual influence of radiolytic oxidants on groundwater redox conditions would be expected to be minor.

It can be concluded that no major perturbation of groundwater redox conditions will occur within a failed container, although there remains the possibility the redox conditions will be slightly more oxidizing inside failed cladding than outside. For pressure tubes, no meaningful perturbation in groundwater redox conditions due to water radiolysis would occur.

5. CORROSION PROCESSES ON ZIRCONIUM ALLOYS

Based on the above discussions, the two processes which could lead to corrosion of Zr alloys (and, for comparison, Ti alloys) are passive film breakdown leading to pitting under oxidizing conditions and hydrogen absorption leading to embrittlement under anoxic to reducing conditions, as illustrated in Figure 18. Also shown on the figure is the range of corrosion potentials (E_{CORR}) measured in a series of neutral pH sulphate, chloride or perchlorate (0.1 mol/L) solutions with the positive potential limit showing the values obtained in aerated solutions and the negative limit those obtained under Ar-purged conditions (Jensen et al. 2002). These values should not be considered definitive since a systematic and comprehensive series of measurements was not performed. A similar range of E_{CORR} values has been observed for Ti alloys (Noël 1999, He 2003).
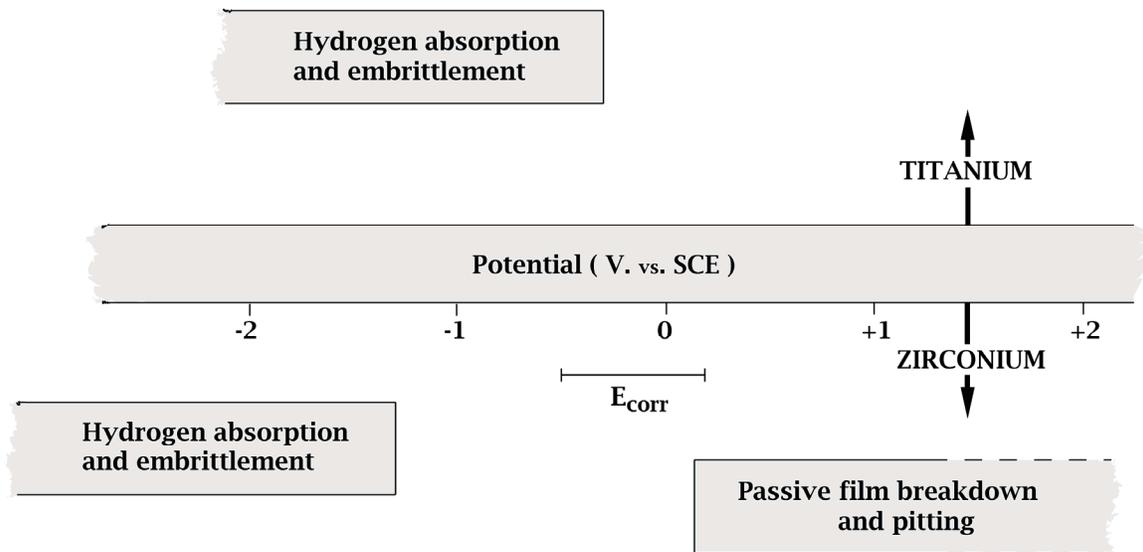
Figure 18: Schematic showing the potential ranges within which passive film breakdown/pitting and H absorption/embrittlement could occur on Ti and Zr alloys. The bar marked E$_{CORR}$, shows the range of corrosion potentials measured on Zr alloys in neutral solution

Since the groundwater entering a failed container will be saline (Table 2), a susceptibility to film breakdown and pitting is possible, providing the environment is sufficiently oxidizing to polarize the E_{CORR} into the potential range of susceptibility, Figure 18. As discussed above, for Zircaloy cladding, the only source of oxidants within a failed container is the fuel radiation field leading to gamma radiolysis products on the outer surface of the cladding and primarily H_2O_2, due to α-radiolysis, on the inner surface. If hydrogen absorption and embrittlement is to occur then E_{CORR} must be polarized to more negative potentials. Cathodic polarization could be achieved if contact with carbon steel was established since this is a base metal with a very low corrosion potential (~ -800 mV vs. SCE) under the anoxic conditions prevailing at steel surfaces within a failed container.
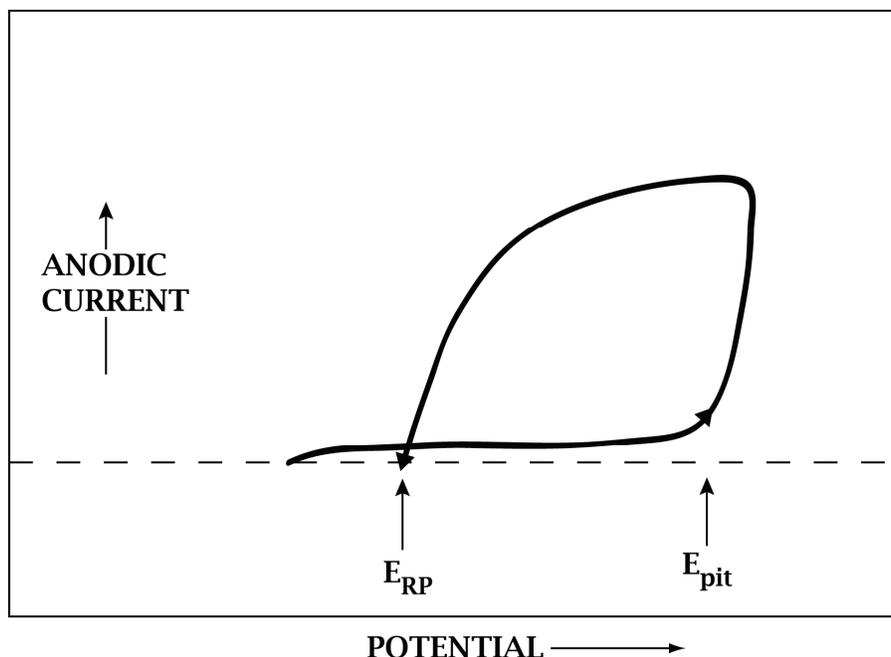
Figure 19: Illustration showing the form of the current-potential relationship observed in a potentiodynamic scan recorded to determine the pitting breakdown potential (E_{pit}) and the repassivation potential (E_{RP})

The corrosion properties of Ti alloys have been reviewed in detail (Hua et al. 2005 a, b) and show that these alloys are very resistant to pitting as expected because of the excellent properties of TiO_2 films under oxidizing conditions (Section 2). Pitting potentials for commercially pure Ti are in excess of 7V and even for β-phase containing alloys are in the region of 2V (Shoesmith and Ikeda 1997). By contrast, the instability of TiO_2 films under cathodic polarization (reducing conditions), especially the films protecting grain boundary precipitates, makes Ti and its alloys susceptible to H absorption and embrittlement when coupled to less noble metals such as carbon steel (Schutz and Thomas 1987, Chung 1993, Hodgkeiss et al. 1987). However, even allowing for this susceptibility, temperatures in excess of 80°C are required before significant damage is incurred.

For Zr and its alloys, the stability of the passive ZrO_2 film under cathodically-polarized conditions rules out any influence of galvanic coupling to reactive metals and there are no reports of Zr alloy degradation under out-of-reactor conditions. Consequently, the possibility of cladding and pressure tube corrosion due to galvanic coupling to the carbon steel container vessel can be dismissed.

Inspection of Figure 18 shows that E_{CORR} for Zr alloys is close to, if not in, the susceptibility region for film breakdown and pitting. Consequently, many researchers have studied the susceptibility of Zr and its alloys to pitting and many values of pitting breakdown and repassivation potentials have been reported (Meisterjahn et al. 1987, Mamun et al. 2001, Knittel et al. 1982, Greene et al. 2000, Fahey et al. 1997, Hornkjol 1988, Maguire 1984, Mankowski et al. 1989, Maguire 1984, Satpati et al. 2005). These potentials are measured using the standard potentiodynamic method in which the potential applied to the material is scanned to positive

values until the pitting breakdown potential (E_{pit}) is surpassed and then back again until the repassivation potential (E_{RP}) is reached, as illustrated in Figure 19. Using this technique, Zr alloys appear susceptible to pitting at very low potentials providing the concentration of chloride is high enough, as shown for two sets of E_{pit} values in Figure 20 (Jangg et al. 1978, Knittel and Bronson 1984). Similar investigations show film breakdown and pitting also occur in bromide and iodide solutions, but only at E_{pit} values well beyond the E_{CORR} range in Figure 18 (Hornkjol 1988).
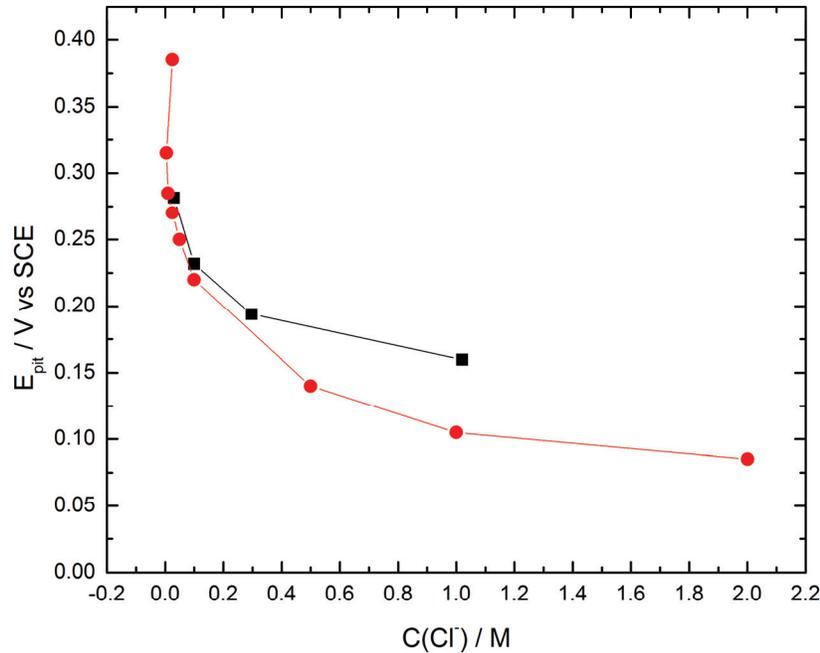
Figure 20: Pitting breakdown potentials recorded as a function chloride concentration (C); ○-Knittel and Bronson (1984); □ Jangg et al. (1978)

The proximity of E_{pit} values in chloride solutions to E_{CORR} values (Figure 18) suggests that Zircaloy cladding could be susceptible to pitting in crystalline rock groundwaters (0.2 mol/L ≤ [Cl⁻] ≤ 1 mol/L; Table 2) and especially in deep sedimentary rock groundwaters (2.7 mol/L ≤ [Cl⁻] ≤ 5.7 mol/L; Table 2). If susceptibilities were to be based on repassivation potentials (E_{RP}), a commonly used conservative approach in corrosion engineering, then pitting would be classed as inevitable since, in many cases, values more negative than the E_{CORR} range in Figure 18 have been reported (Bellanger and Rameau 2000, Gardiazabal 1981, Gómez 1985, Chen et al. 1985, Galvele et al. 1990).

However, the application of the potentiodynamic technique to Zr alloys has many issues and produces results at odds with those based on corrosion experiments and industrial experience. Pitting is only seen under natural corrosion conditions when strong oxidants such as Fe[III] and Cu[II] in acidic solutions and dissolved Cl_2 are present (Schutz and Thomas 1987). Also, recent studies (Satpati et al. 2005) show that the rate at which the potentiodynamic scan is applied

significantly influences the value of E_{pit}. This is not surprising since the rate of film growth under potentiodynamic conditions will be an important determinant of the interfacial stress build-up leading to the introduction of migration pathways which then allow Cl^- ions access to the alloy/oxide interface to cause pit initiation. Surface analytical evidence exists to show that Cl^- ions are incorporated into the anodically growing film in this manner (Schennach et al. 2000). In addition, in potentiostatic experiments in which the applied potential was increased in small steps and then held constant for up to 2 hours, E_{pit} in 0.1 mol/L chloride was ~0.6V (vs. SCE) (Jensen 2002), a value more consistent with corrosion experience. In these last studies no significant differences between Zircaloys and Zr-2.5Nb were observed.

It is clear from this last experiment and from corrosion experience that a sufficient oxidant concentration able to polarize E_{CORR} well beyond the electrochemically determined threshold for pitting susceptibility (Figure 18) is required if pitting is to be initiated and sustained. The only oxidants available within a failed container will be those produced by the radiolysis of water, and, as argued above, the impact of radiolysis on the solution redox potential is expected to be marginal.

This claim that radiolysis will exert a negligible influence on Zr alloy corrosion is supported by a wealth of evidence on radiation effects on the corrosion of passive materials (Shoesmith and King 1999, Landolt et al. 2008). While little data is available for Zr alloys, Ti and its alloys have been well studied. No significant influence of gamma radiation was observed on a number of Ti alloys in a wide range of environments (including Mg-containing saturated brines considerably more aggressive than even the most concentrated sedimentary rock groundwater (SR-300, Table 2) at temperatures up to 250°C. Gamma dose rates in the region of 10^3 Gy/hr did lead to increased corrosion rates and the incorporation of groundwater species, such as Mg^{2+}, into the outer regions of the passive film, but such dose rates are well in excess of the highest radiation dose rates from the fuel, Figure 17.

There is evidence to show that radiation exposure decreases the susceptibility to localized corrosion on both Zircaloy-4 (Bellanger and Rameau 2000) and Ti (Ikeda et al. 1990). A dose rate of ~ 10^2 Gy/hr was clearly shown to inhibit the propagation of crevice corrosion on commercially pure Ti (Grade-2) (Ikeda et al. 1990) which is notoriously susceptible to this form of corrosion (Noël et al. 2001). Since crevice corrosion can initiate and propagate on Ti by a similar mechanism to that for pitting of Zr alloys, and at potentials considerably lower than the measured E_{CORR} values for Zr alloys, a similar influence of radiation on the pitting of cladding would be anticipated. For localized corrosion to occur, anodic (metal dissolution) and cathodic (oxidant reduction) sites must be separately supported on the corroding surface. (In an electrochemical experiment they are artificially separated on different electrodes). By producing oxidants universally across the surface, gamma radiation prevents the stable maintenance of such separated locations.

These conclusions are supported by experiments in which radiation effects were simulated by using solutions containing H_2O_2 (Kim and Oriani 1987; Pan et al. 1994, 1996), a situation similar to that anticipated on the inner cladding surface (Section 4). Although short term increases in corrosion rate were observed they decreased with time as films thickened and became less defective and more protective. No measurable influence of H_2O_2 was observed for concentrations < 5 X 10^{-5} mol/L. At the low radiation dose rates prevailing at the fuel surface, and in the presence of considerable concentrations of the oxidant scavengers, Fe^{2+} and H_2, radiolytic peroxide concentrations would be well below this threshold.

Figure 21 summarizes the influence of gamma radiation on a series of materials studied in a range of neutral saline environments (up to 34,000 mg/L) similar to those anticipated in a crystalline rock repository (Table 2). If Zr cladding were to respond to radiation in a similar manner to Ti alloys then it could be claimed that radiation effects would be negligible. Even if Zr alloys were to perform no better than the more susceptible stainless steels, no significant effect of radiation would be observed beyond a few hundred years, Figure 17, a period well before containers would be expected to fail and allow cladding contact with groundwater.
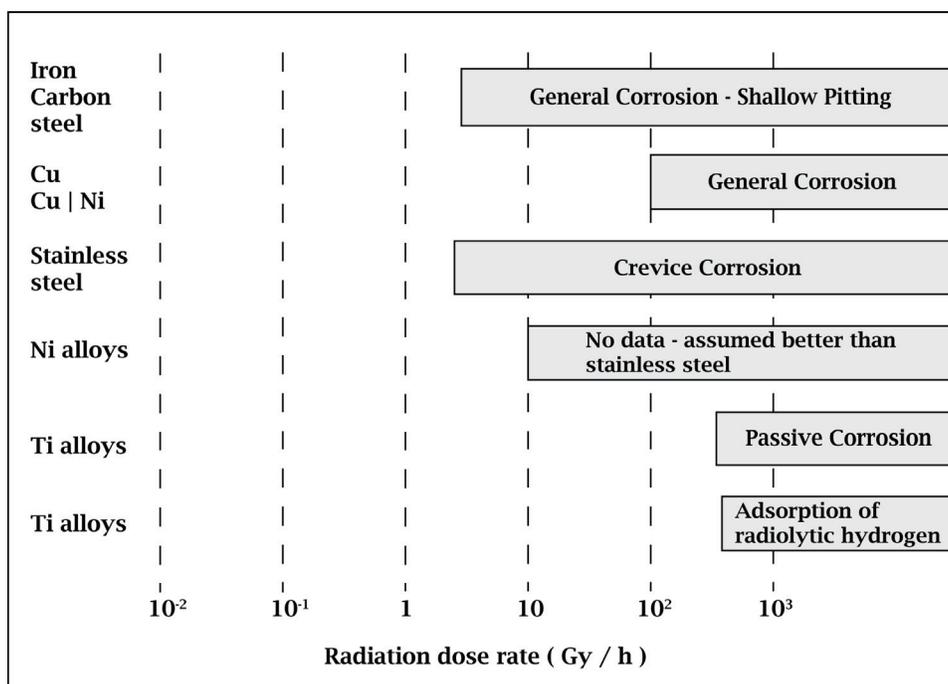
Figure 21: Summary showing the gamma radiation dose rate ranges (shaded areas) within which a measurable influence of radiation on various corrosion processes on various materials has been observed (Shoesmith and King 1999). At dose rates below these regions experiments have revealed no observable radiation effect.

6. PASSIVE CORROSION OF ZIRCONIUM ALLOYS

Based on the above discussion no localized corrosion processes would be expected to occur on Zircaloy cladding leaving passive corrosion as the only feasible mechanism. The generally accepted mechanism for passive corrosion involves a balance between the chemical dissolution rate of the oxide at the oxide/solution interface and the corrosion process to regenerate the oxide at the metal oxide interface, as illustrated schematically for Zr/ZrO_2 in Figure 22. To maintain the passive state, the overall corrosion rate must be controlled by the rate of dissolution at the oxide/solution interface, a process which would be expected to be very slow since the solubility of ZrO_2 in the pH range for groundwaters (~6 to 9) is very low (Baes and Mesmer 1976), Figure 23. Since ZrO_2 is an insulator, such a balance could only be established across a very thin oxide layer since electron transfer to reduce water is required to oxidize the metal/oxide interface.
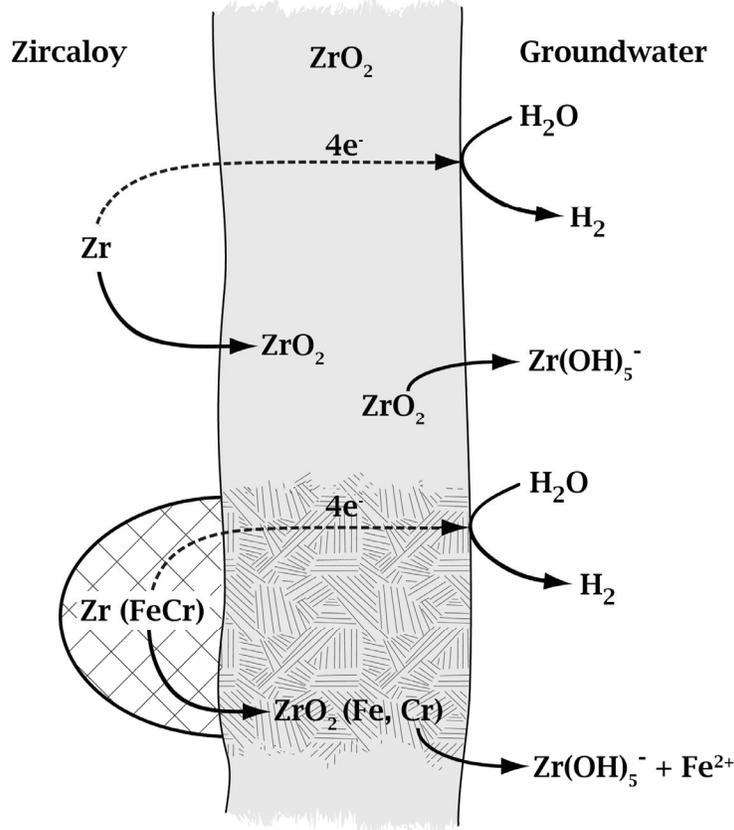
Figure 22: Schematic illustrating the passive corrosion process occurring on a Zr alloy surface. The passive corrosion process involves a steady-state between the rate of chemical dissolution of the oxide at the oxide/groundwater interface and the rate of its regeneration by metal oxidation at the alloy/oxide interface. This requires electron transfer through the oxide to reduce H_2O. Since the oxide associated with corroded SPPs (Zr (Fe, Cr)) could have different properties to that associated with the Zircaloy matrix, the passive corrosion process may temporarily proceed at a different rate at locations involving SPPs. The absence of SPPs in the oxide on Zr-2.5Nb precludes this last feature on pressure tubes.

Segall et al. (1988) have categorized oxides according to their conductivity type and other chemical properties, Figure 24. According to this categorization, ZrO_2, like TiO_2, Al_2O_3 and ThO_2, belongs to the insulating oxide category which dissolves extremely slowly in acidic, and especially neutral, solutions. According to Segall et al. (1988), the mechanism of dissolution of these oxides is surface coordination of the metal cation in the oxide by OH^- ions leading to hydrolysis prior to the breaking of the strong M–O bond and transfer of the hydrolyzed cation ($Zr(OH)_5^-$ in the case of ZrO_2) into solution. For this reason these oxides are more likely to dissolve in alkaline solutions, albeit still very slowly. The dissolution process of oxides in this category are generally insensitive to solution redox conditions since they are unstable in alternative oxidation states to those existing in the oxides, and cannot, therefore, be converted to more soluble states by redox processes. This is in contrast to, say, iron oxides which are

insoluble in the Fe[III] form but considerably more soluble as Fe[II], Figure 16, and uranium oxide (UO_2) which is many orders of magnitude more soluble in the U[VI] than the U[IV] state (Grenthe et al. 1992, Guillamont et al. 2003).
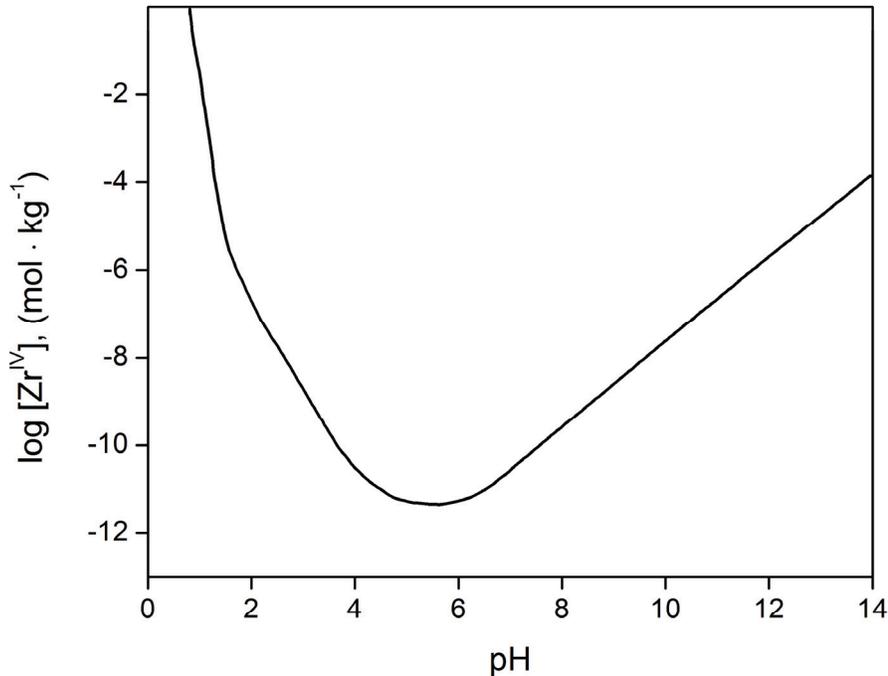
Figure 23: Solubility of Zr as a function of pH (Baes and Mesmer 1976)

While the available measurements on the dissolution rates of oxides on Zr alloys are sparse, a considerable database of passive corrosion rates exists for Ti alloys. According to Segall et al. (1988), the rate of oxide dissolution is dependent on the defect density of the oxide and the creation of surface states that can be neutralized by transfer to the solution. That the rate is dependent on the defect density in the oxide has been clearly demonstrated for NiO, the rate of dissolution varying by two to three orders of magnitude depending on the method of preparation and the subsequent defect annealing temperature (Jones et al. 1977, Pease et al. 1986).

While TiO_2 and ZrO_2 are not included in the same oxide category as NiO, Figure 24, a similar, but independently developed understanding of the passive corrosion of Ti has been published (Hurlen and Hjornkol 1991). It was claimed that the passive corrosion of Ti in neutral solutions was controlled by the migration of the prominent defect (an oxygen vacancy) in the oxide. Since transport in ZrO_2 also involves an oxygen vacancy, a similar dissolution mechanism should prevail. This correlation between defect density in the oxide and its dissolution rate has been clearly established (Blackwood et al. 1988). Since the oxide growth process also utilizes defects (Macdonald 1999) their number density can be influenced by varying the oxide growth rate electrochemically. Oxides grown slowly, and hence possessing a low defect density (Blackwood and Peter 1990), dissolved much more slowly than those with a large defect density due to rapid growth. In addition, with time, films initially grown rapidly (and hence defective)

undergo a defect annealing process which renders them inert to dissolution. Such a defect annealing process is well demonstrated electrochemically for both TiO_2 films (Leitner et al. 1986) and for ZrO_2 films on Zr, Zr-2 and Zr-2.5Nb (Jensen 2002). Also, under natural corrosion conditions, passive corrosion rates for Ti (stimulated by the addition of H_2O_2 to phosphate buffered saline solutions) decrease to very low values with time as the films thicken and defect-anneal (Fonseca and Barbosa 2001).
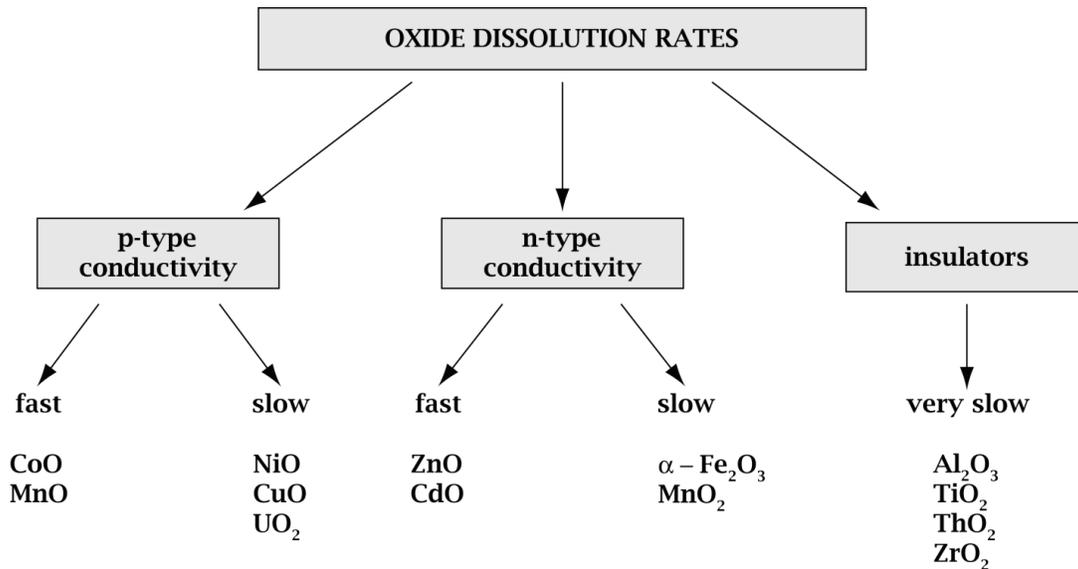
Figure 24: Categorization of the dissolution rates of various oxides separated according to their conductivity type (Segall et al. 1988)

This long term decrease in passive corrosion rates as the oxide thickens and becomes less defective was clearly demonstrated in the Yucca Mountain project for Ti alloys (Hua et al. 2005, Bechtel SAIC 2004). Over a five year period, the rates decreased from ≥ 100 nm/year to between 0 and 20 nm/year, as shown by the distribution of rates for many specimens in Figure 25. The two values > 20 nm/year and the negative corrosion rates shown in this figure probably reflect the uncertainties in making these measurements by weight change methods. These measurements were made in a series of simulated groundwaters at temperatures from 60°C to 90°C and at pH values covering the range 2.7 to 12. The chloride concentrations in the solutions ranged from 67 mg/L to 178,600 mg/L which are comparable with those anticipated in crystalline and sedimentary rock environments (Table 2). No discernible dependence of the rate on temperature, pH or salinity was observed.
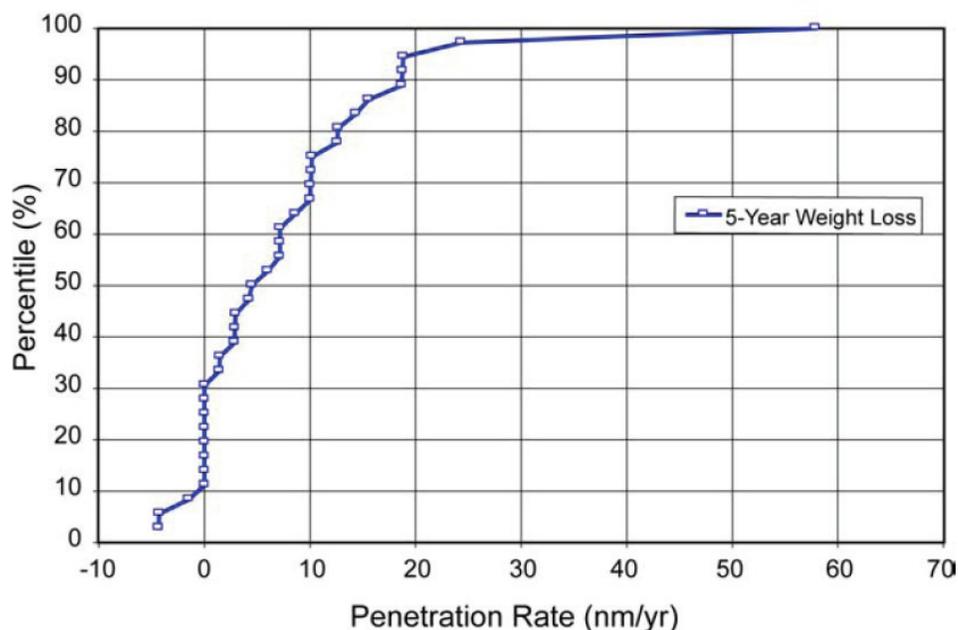
Figure 25: Distribution of the passive corrosion rates of the Pd-containing Ti alloy, Grade-16, measured after exposure to a number of concentrated saline groundwaters (Hua et al. 2005 a, b, c)

These low passive corrosion rates are consistent with a wealth of other measurements made using a range of different techniques. Mattson and Olefjord (1990), using a combination of depth profiling by ion sputtering and X-ray photoelectron spectroscopy (XPS), measured (over a 6 year period) rates in the range 0.5 to 4 nm/year on both commercially-pure (Grade-2) Ti and the Pd-containing Grade-7 in compacted clays saturated with saline solutions at 95°C. Kim and Oriani (1987) measured (over a two year exposure period) rates of 40 to 60 nm/year in $MgCl_2$-dominated brine using ion sputtering and Auger spectroscopy, and found only a marginal increase in rate between 25°C and 108°C (the boiling point of the brine). A similar absence of any temperature dependence (90°C to 200°C) was observed by Smailos et al. (1986, 1987) for Grade-7 Ti in very aggressive German Q-brines (NaCl 4.7%; $MgCl_2$ 26.8%; $MgSO_4$ 1.4%; H_2O 65.7%; pH = 4.9 (at 25°C)) over an exposure period of 3.5 years. Even at 250°C Molecke et al. (1982) found a corrosion rate for Grade-7 Ti of only 400 nm/year in aerated brine. Blackwood et al. (1988) measured rates (at 40°C) on Grade-2 Ti in acidic ($-1 \le pH \le \sim 1$) solutions using electrochemical techniques. Since these last authors also determined a pH-dependence for the corrosion rate it is possible to extrapolate and estimate that the rates in more neutral environments (~pH = 5) should be in the range 15 to 25 nm/year, slightly above the values measured in Yucca Mountain environments (Hua et al. 2005, Bechtel SAIC 2004).

Oxide dissolution rates have been measured on Zr on specimens prepared electrochemically by anodic oxidation. As expected the rates depend very much on the conditions of preparation which control the defect density in the oxide. Dissolution rates were determined using capacitance measurements which allow determination of the change in oxide film thickness with time. The films grown in this manner consist of two layers; an outer hydroxide or hydrated ZrO_2 layer which dissolves rapidly and an inner barrier layer with properties which more closely resemble those of a stable passive film. Figure 26 shows measurements of the dissolution

rates for the inner barrier layer oxide (Mogoda 199a, b; El-Mahdy and Mahmoud 1998; El-Mahdy et al. 1996; Huot 1992; Allah 1989). The irreproducibility of the rates measured in acidic solutions reflects the differences in defect density due to different growth procedures. Even allowing for similar ambiguities over film properties, the dissolution rates measured in neutral solutions are in the range 5 to 20 nm/year, consistent with the range of values obtained for the passive corrosion of Ti. That extremely low to negligible rates can be observed even in very acidic solutions, as shown in Figure 26, has been confirmed by a combination of capacitance and UV-visible interference spectroscopy measurements (Merati and Cox 1999). No measurable dissolution occurred in solutions with pH values in the range -1 to 1 unless fluoride was present. This last study suggests that all the rates plotted in Figure 26 may be conservatively high.
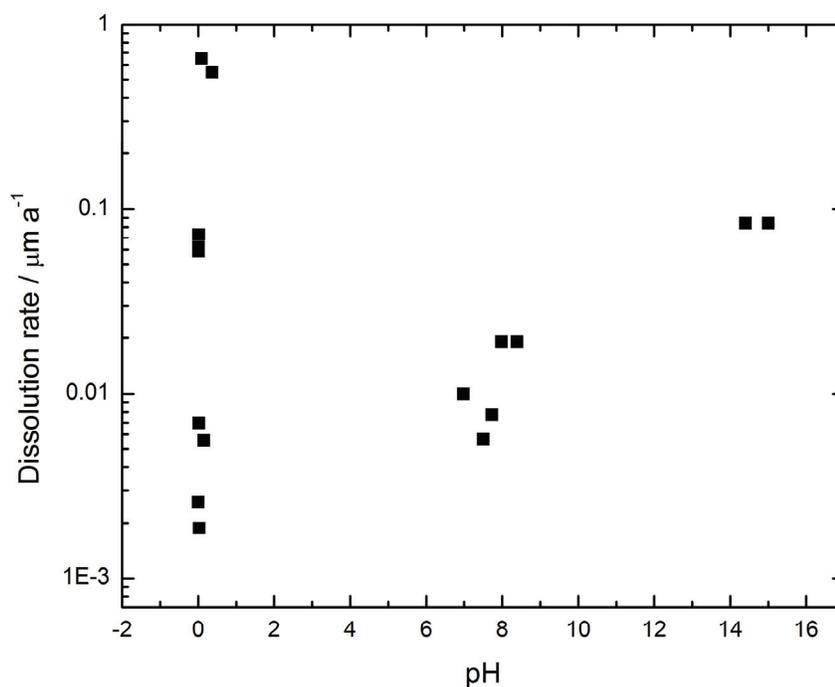
Figure 26: Dissolution (passive corrosion) rates of anodically grown oxides on Zr as a function of pH (Mogoda 1999a, El-Mahdy and Mahmoud 1998, El-Mahdy et al. 1996, Huot 1992, Allah et al. 1989)

This last claim appears to be verified by rates based on measurements of H_2 gas generation for Zr-4 in a seawater-based solution (pH = 10, 12.5; T = 30°C, 50°C) for periods of 180 or > 300 days (Wada et al. 1999). These rates were up to an order of magnitude lower than the values obtained electrochemically and by surface analytical techniques (above). As expected, the rates in these last experiments decreased with exposure time, the weight gain observed indicating some oxide growth. While initially exceeding 1 nm/year, the rate fell to within the range 10^{-1} to 1 nm/year. Given that the rate increases slightly with pH and the solubility of $Zr(OH)_x^{(x-4)-}$ decreases as the pH is lowered, Figure 23, even lower rates might be expected at the pH

prevailing in groundwater. Comparison of these rates to those measured in anaerobic alkaline solutions on Zr-2 (10 nm/year; Hansson 1985) support this claim.

Chemical analyses (Wada et al. 1999) showed the presence of both dissolved Zr and Fe, with the presence of the latter in amounts equal to or greater than the amounts of Zr, suggesting that the corrosion process may have occurred at the locations of secondary phase particles (Zr (Fe, Cr)$_2$) in the Zircaloy matrix. Since in these experiments the secondary phase precipitates would not be covered by the thick oxide present on cladding and pressure tubes, their preferential corrosion would not be surprising. Although not immediately relevant to disposal under anaerobic conditions, very similar corrosion rates (0.1 to 1 nm/year) were obtained in aerated dilute saline solutions (Videm 1981) suggesting a moderate increase in groundwater E_h would not lead to any significant increase in corrosion rate.

The properties of the oxide on Zr cladding, but not that on Zr-2.5Nb pressure tubes, could vary depending on the extent of doping by cations from the corrosion of SPPs, Figure 14. According to Segall et al. (1988) this could lead to an increase in oxide dissolution rate since the oxide at this location would contain a higher concentration of defects in the form of oxygen vacancies. However, while such doping may lead to a slightly enhanced oxide dissolution rate this would not lead to enhanced passive corrosion of the Zircaloy substrate at this location. As discussed above, SPPs oxidize more slowly than the Zr matrix and steady-state passive corrosion would be expected to be slower at these locations, Figure 22.

7. CONCLUSIONS

The corrosion of Zr alloys under deep geological repository conditions has been reviewed. Since the available data base for the corrosion of Ti alloys under repository conditions is more extensive than that for Zr alloys, this has been achieved by comparison of the electrochemical and corrosion behaviour of both alloy series.

This review shows that the oxide film formed in-reactor on Zr alloys is likely to contain ion migration pathways that could allow access of groundwater chloride ions to the alloy/oxide interface, a condition generally associated with pitting corrosion.

However, despite the presence of the radiation fields associated with the fuel, the groundwater redox conditions within a failed waste container will remain reducing, primarily due to the production of the oxidant scavengers, Fe^{2+} and H_2, by corrosion of the steel vessel. Consequently, the only feasible corrosion mode that could lead to degradation of the cladding and pressure tubes is passive corrosion.

Based on a wealth of studies on both Ti and Zr and their alloys a conservative upper limit for the passive corrosion rate would be ~ 20 nm/year. Based primarily on extensive measurements performed within the USA Department of Energy Yucca Mountain project, a value of ~ 5 nm/year would be expected, although some studies exist to show rates < 1 nm/year are likely.

REFERENCES

Ai, J., Y. Chen, M. Urquidi-Macdonald and D.D. Macdonald. 2008. Electrochemical impedance spectroscopic study of passive zirconium. Journal of Nuclear Materials, 379, 162-168.

Allah, A.G., A.A. Mazhar, F.E.T. Heakel and M.A. Ameer. 1989. Formation and dissolution of anodic oxide films on zirconium in NaOH: Kinetic studies. Journal of Applied Electrochemistry, 19, 213-218.

Baes, C. F. and R.E. Mesmer. 1976. The Hydrolysis of Cations. John Wiley and Sons: New York, New York.

Bechtel SAIC Company. 2004. Hydrogen-induced cracking of the drip shield. ANL-EBS-MD-000006. Rev 02. Bechtel SAIC Company: Las Vegas, Nevada.

Been, J. and J.S. Grauman. 2000. Titanium and Titanium Alloys, In: Uhlig's Corrosion Handbook, 2nd Edition, Revie, R.W., editor. Chapter 47. John Wiley: New York, New York.

Bellanger, G. and J. J. Rameau. 2000. Inhibition of chloride pitting corrosion of Zircaloy-4 alloy in highly radioactive water by radiolytic nitrate and hydrogen peroxide. Journal of Materials Science, 35, 1759-1771.

Blackwood, D.J. and L.M. Peter. 1990. Potential modulated reflectance spectroscopy of anodic oxide films on titanium. Electrochimica Acta, 35, 1073-1080.

Blackwood, D.J., C.C. Naish, N. Platts, K.J. Taylor and M.I. Thomas. 1995. The anaerobic corrosion of carbon steel in granite groundwater. Swedish Nuclear Fuel and Waste Management Company Technical Report, TR-95-03. Stockholm, Sweden.

Blackwood, D.J., L.M. Peter and D.E. Williams. 1988. Stability and open circuit breakdown of the passive film on titanium. Electrochimica Acta, 33, 1143-1149.

Casillas, N., S. Charlebois, W.H. Smyrl and H.S. White. 1994. Pitting corrosion of titanium. Journal of Electrochemical Society, 141, 636-642.

Chen, J.S., A. Bronson and D.R. Knittel. 1985. Pitting corrosion on zirconium in KCl and KCl-H_2SO_4 solutions. Corrosion, 41, 438-445.

Cheng, T.-P., J.-R. Lee and W.-T. Tsai. 1993. Galvanic corrosion of titanium-coupled aluminum bronze. Materials Chemistry and Physics, 36, 156-160.

Cox, B. 1968. A porosimeter for determining the sizes of flaws in zirconia or other insulating films "in-situ". Journal of Nuclear Materials, 27, 1-11.

Cox, B. 1969. Rate controlling process during the pretransition oxidation of zirconium alloys. Journal of Nuclear Materials, 31, 48-66.

Cox, B. 1970. Factors affecting the growth of porous anodic oxide films on zirconium. Journal of Electrochemical Society, 117, 654-663.

Cox, B. 1987. Pore structure in oxide films on irradiated and unirradiated zirconium alloys. Journal of Nuclear Materials, 148, 332-343.

Cox, B. and J.P. Pemsler. 1968. Diffusion of oxygen in growing zirconia films. Journal of Nuclear Materials, 28, 73-78.

Cox, B. and C. Roy. 1966. Transport of oxygen in oxide films on zirconium determined by the nuclear reaction $O^{17} (He^3, \alpha) O^{16}$. Electrochemical Technology, 4, 121-127.

Duro, L., M. Grive, E. Cera, X. Gaona, C. Domenech and J. Bruno. 2006. Determination and assessment of the concentration limits to be used in SR-Can. Swedish Nuclear Fuel and Waste Management Company Technical Report, TR-06-32. Stockholm, Sweden.

Elliott, A.J. and D.M. Bartels. 2009. The reaction set, rate constants and g-values for the simulation of radiolysis of light water over the range 20° to 350°C based on information available in 2008. Atomic Energy of Canada Limited Report, 153-127160-450-001. Chalk River, Canada.

El-Mahdy, G.A., S.S. Mahmoud and H.A. El-Dahan. 1996. Effect of halide ions on the formation and dissolution behavior of zirconium oxide. Thin Solid Films, 286, 289-294.

El-Mahdy, G.A. and S.S. Mahmoud. 1998. Effect of Different Acid Anions on Kinetics of the Formation and Dissolution Behavior of Anodic Zirconium Oxide. Corrosion, 54, 354-361.

Fahey, J., D. Holmes and T-L. Yau. 1997. Evaluation of localized corrosion of zirconium in acidic chloride solutions. Corrosion, 53, 54-61.

Fonseca, C. and M.A. Barbosa. 2001. Corrosion behaviour of titanium in biofluids containing H_2O_2 studied by electrochemical impedance spectroscopy. Corrosion Science, 43, 547-559.

Galvele, J.R., R.M. Torresi and R.M. Carranza. 1990. Passivity breakdown and its relation to pitting and stress-corrosion-cracking processes. Corrosion Science, 31, 563-571.

Gardiazabal, I., R. Schrebler, and R. Cordova. 1981. The potentiodynamic behaviour of zirconium and Zircaloy-4 in chloride acid media. Journal of Electroanalytical Chemistry, 119, 389-394.

Garisto, F., T. Kempe and P.Gierszewski. 2009. Technical summary of the safety aspects of the deep geological repository concept for used nuclear fuel. Nuclear Waste Management Organization Technical Report, NWMO TR-2009-12. Toronto, Canada.

Gómez, H., J. Gardiazabal, R. Vera, R. Schrebler ad R. Cordova. 1985. Passivation kinetics of Zircaloy-4 electrode in mineral acids under potentiodynamic conditions. Journal of Electroanalytical Chemistry, 188, 39-48.

Greene, C.A., C.S. Brossia, D.S. Dunn, and G.A. Cragnolino. 2000. Environmental and electrochemical factors on the localized corrosion of Zircaloy-4. Corrosion 2000, Paper No. 002210. NACE International Annual Conference. Houston, Texas.

Grenthe, I., J. Fuger, R.J. Konings, R.J. Lemire, A.B. Muller, C. Nguyen-Trung and H. Wanner. 1992. Chemical Thermodynamics of Uranium, North Holland, Amsterdam.

Guillamont, R., R.T. Fanghanel, I. Grenthe, V. Neck, D. Palmer and M.H. Rand. 2003. Update on the chemical thermodynamics of uranium, neptunium, plutonium, americium and technetium, OECD-NEA, Chemical Thermodynamics, Vol. 5, 182-187, Elsevier, Amsterdam.

Hansson, C.M. 1985. Corrosion of steel and zirconium in anaerobic concrete. Journal Volume 50, 475-482. Conference: Materials Research Society Proceedings International Symposium, Stockholm, Sweden.

Hatano, Y., K. Isobe, R. Hitaka and M. Sugisaki. 1996. Role of intermetallic precipitates in hydrogen uptake of Zircaloy-2. Journal of Nuclear Science and Technology, 33, 944-949.

He, X. 2003. Effects of temperature, impurities, and alloying elements on the crevice corrosion of alpha titanium alloys; Ph.D. Thesis. The University of Western Ontario. London, Ontario, Canada.

Hodgkeiss, T., A. MacIver, and P.Y. Chong. 1987. Galvanic studies related to the use in desalination plant of corrosion-resistant materials. Desalination, 66, 147-170.

Hornkjøl, S. 1988. Pitting corrosion of zirconium and hafnium. Electrochimica Acta, 33, 289-292.

Hua, F., K. Mon, P. Pasupathi, G. Gordon and D.W. Shoesmith. 2005. A review of corrosion of titanium Grade-7 and other titanium alloys in nuclear waste repository environments. Corrosion, 61, 987-1003.

Hua, F., K. Mon, G. De, P. Pasupathi, G. Gordon and D.W. Shoesmith. 2005. Hydrogen induced cracking of titanium alloys in environments anticipated in the Yucca Mountain Nuclear Waste Repository, Corrosion2005, Paper No. 0552, National Association of Corrosion Engineers. Houston, Texas, U.S.A.

Hua, F., K. Mon, G. De, P. Pasupathi, G. Gordon and D.W. Shoesmith. 2005. A review of corrosion of titanium Grade-7 and other titanium alloys in nuclear waste repository environments. Corrosion, 61, 987-1003.

Hua, F., K. Mon, P. Pasupathi, G. Gordon and D.W. Shoesmith. 2005. Modelling the hydrogen-induced cracking of titanium alloys in nuclear waste repository environments. Journal of Metals, 57, 20-26.

Hua, F., K. Mon, P. Pasupathi, G.M. Gordon and D.W. Shoesmith. 2004. Corrosion of Grade-7 and other Ti alloys in nuclear waste repository environments - A review. Corrosion 2004, Paper No. 04689, National Association of Corrosion Engineers. Houston, Texas.

Huot, J.Y. 1992. Electrochemical behavior of zirconium metal and its oxide film in LiOH and HF solutions. Journal of Applied Electrochemistry, 22, 852-858.

Hurlen, T. and S. Hornkjøl. 1991. Anodic growth of passive films on titanium. Electrochimica Acta, 36, 189-195.

Hutchinson, B., B. Lehtinen, M. Limbäck, M. Dahlbäck. 2007. A study of the structure and chemistry of Zircaloy-2 and the resulting oxide after high temperature corrosion. Journal of ASTM International (JAI), 4 (10). (Available on-line at: www.astm.org)

IAEA. 1998. Waterside Corrosion of Zirconium Alloys in Nuclear Power Plants. International Atomic Energy Agency Technical Document, IAEA-TECDOC-996, IAEA. Vienna, Austria.

Ikeda, B.M., M.G. Bailey, C.F. Clarke and D.W. Shoesmith. 1990. Crevice corrosion and hydrogen embrittlement of titanium Grades-2 and -12 under Canadian waste vault conditions, In: "Corrosion of Nuclear Waste Containers: Proceedings of a Workshop", edited by D.W. Shoesmith, Atomic Energy of Canada Limited Report, AECL-10121, pp 45-66. Chalk River, Canada.

Ito, Y. and T. Furuya. 1996. Correlation between electrochemical properties and corrosion resistance of zirconium alloys. In: Zirconium in the Nuclear Industry: Eleventh International Symposium, ASTM STP 1295, E.R. Bradley and G.P. Sabol, Eds. American Society for Testing and Materials, 163-180.

Jangg, G., R.T. Webster, and M. Simon. 1978. Investigation into corrosion behavior of zirconium alloys. IV. Pitting behavior of zirconium alloys. Werkst. Korros, 29, 16-26.

Jarzebski, Z.M. 1973. Oxide semiconductors. International Series of Monographs in Science of the Solid-State Vol. 4. Pergamon Press: New York, New York.

Jensen, H. 2002. Properties of anodic oxide films on zirconium alloys, Ph.D. Thesis, The University of Western Ontario. London, Ontario Canada.

Jones, C.F., R.L. Segall, R.St.C. Smart and P.S. Turner. 1977. Semiconducting oxides: the effect of prior annealing temperature on dissolution kinetics of NiO. Journal of Chemical Society, Faraday, Transactions 1, 73, 1710-1720.

Jonsson, M., F. Nielsen, O. Roth, E. Ekeroth, S. Nilsson and M.M. Hossain. 2007. Radiation induced spent nuclear fuel dissolution under deep repository conditions. Environmental Science and Technology, 41, 7087-7093.

Khalil, N. and J.S.L. Leach. 1986. The anodic oxidation of valve metals—1. Determination of ionic transport numbers by α-spectrometry. Electrochimica Acta, 31, 1279-1285.

Kim, Y.J. and R.A. Oriani. 1987. Brine radiolysis and its effect on the corrosion of Grade-12 titanium. Corrosion, 43, 92-97.

Kim, Y.J. and R.A. Oriani. 1987. Corrosion properties of the oxide film formed on Grade-12 titanium in brine under gamma radiation. Corrosion, 43, 85-91.

King, F. 2007. Status of Understanding of Used Fuel Container Corrosion Processes — Summary of Current Knowledge and Gap Analysis, Nuclear Waste Management Organization Technical Report NWMO-TR-2007-09. Toronto, Canada.

Knittel, D.R. and A. Bronson. 1984. Pitting corrosion on zirconium--A review. Corrosion, 40, 9-13.

Knittel, D.R., M. A. Maguire, A. Bronson and J-S. Chen. 1982. The effect of surface treatments and electrochemical methods on the pitting potential of zirconium in chloride solutions. Corrosion, 38, 265- 273.

Landolt, D., A. Davenport, J. Payer and D.W. Shoesmith. 2008. A review of materials and corrosion issues regarding canisters for disposal of spent fuel and high level waste in Opalinus Clay. Nagra Technical Report NTB-09-02, Wettingen, Switzerland.

Leach, J.S.L. and B.R. Pearson. 1988. Crystallization in anodic oxide films. Corrosion Science, 28, 43-56.

Lee, C.T., Z. Qin, M. Odziemkowski, and D.W. Shoesmith. 2005. The influence of groundwater anions on the impedance behaviour of carbon steel corroding under anoxic conditions. Electrochimica Acta, 51, 1558-1568.

Leitner, K., J.W. Schultze and U. Stimming. 1986. Photoelectrochemical investigations of passive films on titanium electrodes. Journal of Electrochemical Society, 133, 1561-1568.

Little, R., J. Avis, N. Calder, N. Garisto, P. Humphreys, F. King, L. Limer, R. Metcalf, J. Penfold, J. Rees, D. Savage, P. Suckling, G. Towler, R. Walke and R. Walsh. 2009. Postclosure safety assessment (V1) report. Nuclear Waste Management Report NWMO DGR-TR-2009-01. Toronto, Canada.

Maak, P. 2007. Development of a used fuel container for nuclear fuel waste; Materials Research Society Symposium Proceedings, 807, 447-451

Macdonald, D.D. 1999. Passivity-the key to our metals-based civilization. Pure and Applied Chemistry, 71, 951-978.

Maguire, M. 1984. The pitting susceptibility of zirconium in aqueous Cl^-, Br^- and I^- solutions. Industrial Applications of Titanium and Zirconium: Third Conference, ASTM STP 830, R.T. Webster and C.S. Young, Eds. American. Society for Testing and Materials, pp. 175-189.

Mamun, A., R. Schennach, J.R. Parga, M.Y.A. Mollah, M.A. Hossain and D.L. Cocke. 2001. Passive film breakdown during anodic oxidation of zirconium in pH 8 buffer containing chloride and sulfate. Electrochemica Acta, 46, 3343-3350.

Mankowski, G., Y. Roques and F. Dabosi. 1989. Effect of passive film growth on the kinetics of pit generation on Zircaloy-4. Materials Science Forum, 44-45, 279-288.

Mattsson, H. and I. Olefjord. 1990. Analysis of oxide formed on Ti during exposure in bentonite clay-I, The oxide growth, Werkstoffe and Korrosion, 41, 383-390.

McMurry, J., D.A. Dixon, J.D. Garrroni, B.M. Ikeda, S. Stroes-Gascoyne, P. Baumgartner and T.W. Melnyk. 2003. Evolution of a Canadian deep geologic repository: base scenario. Ontario Power Generation Report 06819-REP-01200-10092-R00. Toronto, Canada.

Meisterjahn, P., H.W. Hoppe and J.W. Schultze. 1987. Electrochemical and XPS measurements on thin oxide films on zirconium. Journal of Electroanalytical Chemistry, 217, 159-185.

Merati, A. and B. Cox. 1999. Dissolution of anodic zirconium dioxide films in aqueous media. Corrosion, 55, 388-396.

Mogoda, A.S. 1999a. Electrochemical behavior of zirconium and the anodic oxide film in aqueous solutions containing chloride ions. Thin Solid Films, 357, 202-207.

Mogoda, A.S. 1999b. Influence of some parameters on passivation of zirconium and the stability of the anodic oxide film. Corrosion, 55, 877-882.

Molecke, M.A., J.A. Ruppen and R.B. Diegle. 1982. Materials for high-level canister/overpacks in salt formations, Sandia National Laboratory Report SAND 82-0429.

Noël, J.J. 1999. The electrochemistry of titanium corrosion. Ph.D Thesis. The University of Manitoba, Winnipeg, Manitoba.

Noël, J.J., D.W. Shoesmith and B.M. Ikeda. 2001. Crevice Corrosion of Alpha Titanium alloys, In: Proceedings of the Research Topical Symposia, NACE Corrosion/2001, Houston, Texas, March 11-16, 2001 (G.S. Frankel and J.R. Scully, Eds.), NACE International, Houston, Texas, 65-102.

Noël, J.J., D.W. Shoesmith and Z. Tun. 2008. Anodic oxide growth and hydrogen absorption on Zr in neutral aqueous solution: A comparison to Ti. Journal of Electrochemical Society, 155, C444-C454.

Noël, J.J., H.L. Jensen, Z. Tun and D.W. Shoesmith. 2000. Electrochemical modification of the passive oxide layer on Zr-2.5Nb observed by in-situ neutron reflectrometry. Electrochemical and Solid-State Letters, 3, 473-476.

Nowierski, C., J.J. Noël, D.W. Shoesmith and Z. Ding. 2009a. Correlating surface microstructures with reactivity on commercially pure zirconium using scanning electrochemical microscopy and scanning electron microscopy. Electrochemistry Communication, 11, 1234-1236.

Nowierski, C. 2009b. Analysis of the electrochemistry and surface microstructure of zirconium alloys under cathodic polarization. M.Sc. Thesis, The University of Western Ontario, London, Ontario, Canada.

Ohtsuka, T., M. Masuda and N. Sato. 1987. Cathodic reduction of anodic oxide films formed on titanium. Journal of Electrochemical Society, 134, 2406-2410.

Ortega, C. and J. Siejka. 1982. A study by nuclear microanalysis and ^{18}O tracing of the growth of anodic oxide films on zirconium. Journal of Electrochemical Society, 129, 1905-1917.

Pan, J., D. Thierry and C. Leygraf. 1994. Electrochemical and XPS studies of titanium for biomaterial applications with respect to the effect of hydrogen peroxide. Journal of Biomedical Materials Research Part A, 28, 113-122.

Pan, J., D. Thierry and C. Leygraf. 1996. Hydrogen peroxide toward enhanced oxide growth on titanium in PBS solution: Blue coloration and clinical relevance. Journal of Biomedical Materials Research Part A, 30, 393-402.

Pease, W.R., R.L. Segall, R.St.C. Smart and P.S. Turner. 1986. Comparative dissolutions rates of defective nickel oxides from different sources. Journal of Chemical Society, Faraday, Transactions 1, 82, 759-766.

Satpati, A.K., S.V. Phadnis and R.I. Sundaresan. 2005. Electrochemical and XPS studies and the potential scan rate dependent pitting corrosion behavior of Zircaloy-2 in 5% NaCℓ solution. Corrosion Science, 47, 1445-1458.

Schennach, R., A. Mamun, N. Kunamneni and D.L. Cocke. 2000. Cyclic voltammetry, x-ray photoelectron spectroscopy, secondary-ion-mass spectrometry, and ion-scattering spectrometry examination of zirconium passive film breakdown in the presence of sulfate. Journal of Vacuum Science and Technology A, 18, 1478-1483.

Schutz R.W. and D.E. Thomas. 1987. Corrosion of Titanium and Titanium Alloys. In: Corrosion, 13, 669-706, ASM Metals Handbook.

Segall, R.L., R.St.C. Smart and P.S. Turner. 1988. Oxide Surfaces in Solution, In: Surface and Near Surface Chemistry of Oxide Materials, edited by J. Nowotny and L.-C. Dufour, Elsevier Science Publishers, Amsterdam, Chapter 13, 527-576.

Shaltiel, D., I. Jacob and D. Davidov. 1977. Hydrogen absorption and desorption properties of AB$_2$ Laves-phase pseudobinary compounds, Journal of the Less-Common Metals, 53, 117-131.

Shibata, T. and Y.-C. Zhu. 1995. The effect of film formation conditions on the structure and composition of anodic oxide films on titanium. Corrosion Science, 37, 253-270.

Shoesmith, D.W. 2006. Assessing the corrosion performance of high-level nuclear waste containers. Corrosion, 62, 703-722.

Shoesmith, D.W. 2008. The role of dissolved hydrogen on the corrosion/dissolution of spent nuclear fuel. Nuclear Waste Management Organization Technical Report NWMO-TR-2008-19. Toronto, Canada

Shoesmith, D.W. and B.M. Ikeda. 1997. The resistance of titanium to pitting, microbially induced corrosion, and corrosion under unsaturated conditions. Atomic Energy of Canada Limited Report AECL-11709, COG-96-557-I. Chalk River, Canada.

Shoesmith, D.W. and F. King. 1999. The effects of gamma radiation on the corrosion *of* candidate materials for the fabrication of nuclear waste packages, Atomic Energy *of* Canada Limited Report, AECL-11999. Chalk River, Canada.

Shoesmith, D.W. and J.J. Noël. 2010. Corrosion of titanium and its alloys, In: Shreir's Corrosion, Richardson, J.A. et al. editors, Vol. 3, 2042-2052. Elsevier, Amsterdam.

Smailos, E. and R. Koster. 1987. Corrosion studies on selected packaging materials for disposal of high level wastes. In: "Materials Reliability in the Back End of the Nuclear Fuel Cycle. International Atomic Energy Agency TECDOC-421, 7-24. IAEA, Vienna, Austria.

Smailos, E., W. Schwarzkopf and R. Koster. 1986. Corrosion behavior of container materials for disposal of high-level wastes in rock salt environments, Nuclear Science and Engineering, Commission of the European Communities, Luxembourg, EUR-10400-EN.

Smart, N.R., D.J. Blackwood and L. Werme. 2002a. Anaerobic corrosion of carbon steel and cast iron in artificial groundwaters: Part 1 - Electrochemical aspects; Corrosion, 58, 547-559.

Smart, N.R., D.J. Blackwood and L. Werme. 2002b. Anaerobic corrosion of carbon steel and cast iron in artificial groundwaters: Part II - Gas generation; Corrosion, 58, 627-637.

Tait, J.C., H. Roman and C.A. Morrison. 2000. Characteristics and radionuclide inventories of used fuel from OPG nuclear generating stations, Volumes 1 and 2. Ontario Power Generation Report 06819-REP-01200-10029-R00. Toronto, Canada.

Torresi, R.M., O.R. Cámara, C.P. DePauli and M.C. Giordano. 1987. Hydrogen evolution reactions on anodic titanium oxide films. Electrochimica Acta, 32, 1291-1301.

Truant, P.T. 1983. CANDU fuel performance: power reactor experience. Atomic Energy of Canada Limited Report AECL-MISC-250 (Rev 1). Chalk River, Canada.

Tun, Z., J.J. Noël, and D.W. Shoesmith. 1999. Electrochemical modification of the passive oxide layer on a Ti film observed by in-situ neutron reflectometry. Journal of Electrochemical Society, 146, 988-994.

Videm, K. 1981. Corrosion studies of candidate materials for permanent storage of nuclear waste, In: Proceedings of International Congress on Metallic Corrosion (8th) Mainz, Germany.

Wada, R., T. Nishimura, K. Fujiwara, M. Tanabe and M. Mihara. 1999. Experimental study on hydrogen gas generation rate from corrosion of Zircaloy and stainless steel under anaerobic alkaline conditions, Radioactive Waste Management and Environmental Remediation — ASME American Society for Mechanical Engineering, Fairfield, New Jersey.

Wersin, P., L.H. Johnson, B. Schwyn, U. Berner and E. Curti. 2003. Redox conditions in the near field of a repository for SF/HLW and ILW in Opalinus clay. Nagra Technical Report 02-13. Wettingen, Switzerland.

Yilmazbayhan, A., E. Breval, A.T. Motta and R.J. Comstock. 2006. Transmission electron microscopy examination of oxide layers formed on Zr alloys. Journal of Nuclear Materials, 349, 265-281.

Zeng, Y. 2009. Passive film properties and their influence on hydrogen absorption into titanium. Ph.D. Thesis, University of Western Ontario, London, Canada.

Zhu, R., C. Nowierski, Z. Ding, J. J. Noël, and D. W. Shoesmith. 2007. Insights into grain structures and their reactivity on Grade-2 Ti alloy surfaces by scanning electrochemical microscopy, Chemistry of Materials, 19, 2533-2543.

Zhu, R., Z. Qin, J. J. Noël, D. W. Shoesmith, and Z. Ding. 2008. Analyzing the influence of alloying elements and impurities on the localized reactivity of titanium Grade-7 by scanning electrochemical microscopy. Analytical Chemistry, 80, 1437-1447.